bioRxiv preprint doi: https://doi.org/10.1101/787077; this version posted September 30, 2019. The copyright holder for this preprint (which was not certified by peer review) is the author/funder, who has granted bioRxiv a license to display the preprint in perpetuity. It is made available under aCC-BY-NC-ND 4.0 International license.

Article

The genome of Mekong tiger perch *(Datnioides undecimradiatus)* provides insights into the phylogenic position of Lobotiformes and biological conservation

Shuai Sun[1,2,3†], Yue Wang[1,2,3,†], Xiao Du[1,2,3,†], Lei Li[1,2,3,4,†], Xiaoning Hong[1,2,3,4], Xiaoyun Huang[1,2,3], He Zhang[1,2,3], Mengqi Zhang[1,2,3], Guangyi Fan[1,2,3], Xin Liu[1,2,3,*], Shanshan Liu[1,2,3*]

[1] BGI-Qingdao, BGI-Shenzhen, Qingdao, 266555, China
[2] BGI-Shenzhen, Shenzhen, 518083, China
[3] China National GeneBank, BGI-Shenzhen, Shenzhen, 518120, China
[4] School of Future Technology, University of Chinese Academy of Sciences, Beijing 101408, China

[†] These authors contributed equally to this work.
[*] Correspondence authors: liushanshan@genomics.cn (S. L.), liuxin@genomics.cn (X. L.)

Abstract

Mekong tiger perch (*Datnioides undecimradiatus*) is one ornamental fish and a vulnerable species, which belongs to order Lobotiformes. Here, we report a ~595 Mb *D. undecimradiatus* genome, which is the first whole genome sequence in the order *Lobotiformes*. Based on this genome, the phylogenetic tree analysis suggested that *Lobotiformes* and *Sciaenidae* are closer than Tetraodontiformes, resolving a long-time dispute. We depicted the pigment synthesis pathway in Mekong tiger perch and result confirmed that this pathway had evolved from the shared whole genome duplication. We also estimated the demographic history of Mekong tiger perch, showing the effective population size suffered a continuous reduction possibly related to the contraction of immune-related genes. Our study provided a reference genome resource for the *Lobotiformes*, as well as insights into the phylogeny of Eupercaria and biological conservation.

Instruction

Mekong tiger perch *(Datnioides undecimradiatus*) *[1]* is one tropical freshwater fish, belonging to the order Lobotiformes under series Eupercaria. It is native to Mekong river and usually found in the main waterway and large tributaries of the Mekong

bioRxiv preprint doi: https://doi.org/10.1101/787077; this version posted September 30, 2019. The copyright holder for this preprint (which was not certified by peer review) is the author/funder, who has granted bioRxiv a license to display the preprint in perpetuity. It is made available under aCC-BY-NC-ND 4.0 International license.

35 river basins, feeding on small fishes and shrimps [2]. It is also one ornamental fish,
36 which is kept for its vertical yellow and black stripes running its body.

37

38 Eupercaria is by far the largest series of percomorphs with more than 6,600 species
39 arranged in 161 families and at least 16 orders. The phylogenetic relationship of the
40 order Lobotiformes, Tetraodontiformes, and the family Sciaenidae is in conflict.
41 Mirande reported Sciaedidae as the sister clade of Tetraodontiformes, and then
42 followed by Lobotiformes based on 44 DNA makers from uncompleted nuclear and
43 mitochondrial sequences combined with morphological characters [3]. Compared to it,
44 Betancur-R et al. reported Lobotiformes was more closely related to
45 Tetraodontiformes than Sciaedidae using molecular and genomic data, which was also
46 not complete or whole-genome sequenced for most of species. [4], agreed with this
47 phylogeny by investigating. However, more recently Lobotiformes was reported to be
48 more closely related to Sciaenidae than Tetraodontiformes based on complete
49 mitochondrial genome [5]using and transcriptomic data [6]. Furthermore, fourteen
50 families of Eupercaria included in order-level *incertae sedis*, which are called "new
51 bush at the top", were not arranged to explicit orders and interrelationships among
52 them was a long-term issue [7]. Therefore, the whole-genome containing
53 comprehensive evolutionary information is called for resolving the long-time dispute
54 on the phylogenetic relationships of the huge number of species in Eupercaria,
55 especially for the problem of "new bush at the top".

56

57 In addition to its evolutionary importance, Mekong tiger perch has a body color
58 pattern with vertical yellow and black stripes. Body color diversity in animals has
59 important functions in numerous biological processes and social behaviors, such as
60 sexual selection, kin recognition and changing coloration for camouflage [8]. Recent
61 studies proposed that teleost genomes might contain more copies of genes involved in
62 pigment cell development than tetrapod genomes after an ancient fish-specific
63 genome duplication (FSGD), which might contribute to the evolution and
64 diversification of the pigmentation gene repertoire in teleost fish [9]. With more
65 genome sequences, especially for fish with unique body color schemes such as
66 Mekong tiger perch, we can further apply comparative genomics to illustrate the

bioRxiv preprint doi: https://doi.org/10.1101/787077; this version posted September 30, 2019. The copyright holder for this preprint (which was not certified by peer review) is the author/funder, who has granted bioRxiv a license to display the preprint in perpetuity. It is made available under aCC-BY-NC-ND 4.0 International license.

genetic mechanisms of body color development.

Mekong tiger perch is currently assigned as 'Vulnerable' due to the rapidly declined population size by the IUCN [10], and is considered as endangered (EN) by Thailand Red data [2]. The external factors, such as the construction of hydraulic engineering infrastructures, urban pollution, and the aquarium trade, are thought to be exerting a negative effect on wild populations. Meanwhile, internal genetic factors such as resistance to biological and abiotic stress may be related to their survivals. Due to its limited distribution and commercial values, rare genetic research has been focused on Mekong tiger perch. With the rapid development of genomics, each fish deserves the right to own its genome assembly representing its unique genetic resource, which will help to better investigate its unique characters and biological conservations.

Here, we sequenced Mekong tiger perch and assembled a reference genome, which was the first genome of the order Lobotiformes. We constructed a phylogenetic tree in Eupercaria based on the whole genome sequences, to elucidate the relationships among family Sciaenidae, order Lobotiformes and order Tetraodontiformes, providing insights into the phylogenic position of Lobotiformes. Utilizing the assembled genome, we identified genes involved in the cell development regulation and pigment synthesis in Mekong tiger perch. We confirmed population decline by the analysis of demographic history and found the contraction of immune-related genes might be a contributing factor for Mekong tiger perch's vulnerability. The genome assembly of Mekong tiger perch provided a valuable genome resource for future fish studies in Lobotiformes, and also contributes to the understanding of body color development as well as demographic history and conservation.

Results

Genome assembly, annotation, and genomic features

We sampled muscle tissue from a Mekong tiger perch captured in Mekong river (**Supplementary Fig. 1**), and applied single tube long fragment read (stLFR) [11]

bioRxiv preprint doi: https://doi.org/10.1101/787077; this version posted September 30, 2019. The copyright holder for this preprint (which was not certified by peer review) is the author/funder, who has granted bioRxiv a license to display the preprint in perpetuity. It is made available under aCC-BY-NC-ND 4.0 International license.

technology for whole genome sequencing, generating stLFR co-barcode reads 122.4 Gb raw data. After filtering low-quality and duplicated reads, we obtioned75.3 Gb clean data for genome assembly using supernova [12], and gaps were closed using GapCloser [13]. We obtained a final genome assembly spanning 595 Mb, accounting for 95.5% of the estimated genome size (623 Mb, **Supplementary Fig. 2**). The assembly achieved a high level of contiguity, with a total of 4,959 scaffolds and scaffold N50 of 9.73Mb. The longest 71 scaffolds (longer than 1.41 Mb) accounted for 90% of the total genome, and the longest scaffold reached up to 39.31 Mb (**Fig. 1**, **Table 1 and Supplementary table 1**). Total repeat content accounted for 11.97% (**Table 1 and Supplementary table 2**) of the genome, and 29,150 protein-coding genes were predicted via *ab initio* and homology-based methods (**Table 1**). The average length of coding sequences (CDS) was 1,510 bp with an average of 9 exons per gene, which were similar to that of other related species (**Supplementary table 3 and Supplementary Fig. 3**). The ncRNAs including miRNA, tRNA, rRNA, and snRNA were also annotated with a total length of 179 kb (**Supplementary table 4**). We used BUSCO metazoan database (v9) to evaluate the completeness of gene sets and observed a completeness of 95.34%. Other databases including Actinopterygii (v9) and vertebrata (v9) estimated the completeness to be 94% and 91%, separately (**Supplementary Fig. 4**). Furthermore, the mitochondrial genome was assembled a total length of 16,606 bp, containing 18 coding genes, 2 rRNA, and 17 tRNA (**Supplementary table 5**).

CpG islands (CGIs) are an important group of CpG dinucleotides in the guanine- and cytosine rich regions as they harbor functionally relevant epigenetic loci for whole genome studies. 32,148 CpG islands (CGIs) were identified with a total length up to 18.8 Mb. The CpG density has the most prominent correlations with three other genomic features. It correlated positively with CG content density and gene density, and correlated negatively with repeat density (**Fig. 1b and Supplementary table 6**), showing a similar pattern observed in other published fishes or mammal [14-16].

bioRxiv preprint doi: https://doi.org/10.1101/787077; this version posted September 30, 2019. The copyright holder for this preprint (which was not certified by peer review) is the author/funder, who has granted bioRxiv a license to display the preprint in perpetuity. It is made available under aCC-BY-NC-ND 4.0 International license.

Phylogenetic tree of Eupercaria uncovers the phylogenetic position of Lobotiformes

To clarify the evolutionary relationships of major orders in Eupercaria clade, 9 sequenced species from 7 different orders were used in the comparative genomics analysis (**Supplementary table 7**). We clustered the gene families based on protein sequences similarity and obtained a total of 13,785 gene families, 1,428 of which were single-copy gene families (**Supplementary Fig. 5 and Supplementary table 8**). The nucleotide sequences on the four-fold degenerate (4d) site of those single-copy gene families were used to construct the maximum likelihood (ML) tree. The phylogeny of the seven orders was found consistent with the previous study [5, 6]. Order Perciformes was identified as the early branch to other orders in Eupercaria, and the divergent time was estimated 101.9 million years ago (mya). Our phylogenetic tree (**Fig. 2a**) showed Lobotiformes was more related to Sciaenidae than to Tetraodontiformes, which supported the results of some previous studies [5, 6]. Furthermore, the divergence time between Lobotiformes and Sciaenidae was inferred to be 82.9 mya (**Fig 2a**).

The conserved genomic synteny reflects the arrangements on evolutionary processes was used to further demonstrate the ambiguous phylogeny among Lobotiformes and closely related orders. The syntenic analysis both at whole-genome nucleotide-level and gene-level were performed by aligning *L. crocea* and *T. rubripes* to our assembled *D. undecimradiatus*, separately. At whole-genome nucleotide-level after filtering alignment length < 1kb, 41.76 % of *D. undecimradiatus* genome sequences were covered by *L. crocea* genome with an average of 2.29 kb per block. In comparison, only 10.48% of *D. undecimradiatus* genome sequences were covered by *T. rubripes* genome with an average of 1.65 kb per block (**Fig. 2b and Supplementary table 9**). Similarly, at the whole genes level after keeping block length > 3 genes, 89.19% of *D. undecimradiatus* genes showed synteny with *L. crocea* with an average of 50.28 genes per block, and 77.21% of *D. undecimradiatus* genes had synteny with *T. rubripes* with an average of 41.28 genes per block (**Fig. 2c and Supplementary table 10**). Despite the difference in genome size, both *L. crocea* and *T. rubripes* genomes were assembled to comparable chromosome level and the

bioRxiv preprint doi: https://doi.org/10.1101/787077; this version posted September 30, 2019. The copyright holder for this preprint (which was not certified by peer review) is the author/funder, who has granted bioRxiv a license to display the preprint in perpetuity. It is made available under aCC-BY-NC-ND 4.0 International license.

BUSCO assessments showed no significant differences in the completeness of genome and gene set between *L. crocea* and *T. rubripes* (**Supplementary table 11**). In addition, the distribution of the length of syntenic blocks at both whole-genome nucleotide-level and gene-level showed significant difference by t-test statistics (nucleotide-level, p-value<0.0001; gene-level, p-value<0.05) (**Supplementary Fig. 6**). Therefore, the results of synteny suggested that the Lobotiformes had better evolutionary conservation and closer relationship with Sciaenidae than with Tetraodontiformes, providing strong evidence for the constructed phylogenic tree.

To further demonstrate the phylogeny among Lobotiformes, Sciaenidae, and Tetraodontiformes, only the homologous genes of 1:1:1 on the syntenic blocks were inferred as reliable orthologous genes to construct the genes genealogy, with the human CDS sequences as outgroup in the rooted tree. 73% of the 3,974 orthologous gene sets supported that *D. undecimradiatus* was more closely related to *L. crocea*, supporting Lobotiformes as sister group to Sciaenidae, instead of the other two hypotheses (**Fig. 2d**).

The genes involved in pigment development and two copies of three rate-limiting genes of pigment synthesis as the result of FSGD similar to other teleosts

In consideration of special skin color pattern, among established pigmentation database containing 198 genes [17], 172 genes were found on our genome, occupying 92% of the database and possibly genetic basis for the phenotypic characteristics of vertical yellow and black stripes running its body (**Supplementary table 12**). For two major pigment synthesis pathways in *D. undecimradiatus*, three main rate-limiting genes of Tyrosinase family (*TYR*, *DCT*, *TYRP1*) in the melanin synthesis pathway have two copies respectively (**Fig.3a**) and one main rate-limiting gene SPR in pteridine synthesis pathway also have two copies (**Fig. 3b**). This suggests *D. undecimradiatus* retained the pigment related genes from a fish-specific whole-genome duplication (FSGD), which was also observed in many other teleosts. It should be noted that the phylogeny of those genes also served as another evidence to the evolution relationship among the three close relative orders.

bioRxiv preprint doi: https://doi.org/10.1101/787077; this version posted September 30, 2019. The copyright holder for this preprint (which was not certified by peer review) is the author/funder, who has granted bioRxiv a license to display the preprint in perpetuity. It is made available under aCC-BY-NC-ND 4.0 International license.

Decreasing population size related to the contraction of immune-related gene families provides clues to biological conservation

Pairwise sequentially Markovian coalescent (PSMC) was used to infer the demographic history of Mekong tiger perch. The effective population size continuously reduced since LGM (last glacial maximum), and there were no signs of recovery to date, which was consistent with its vulnerable state [2, 10](**Fig. 4a**).

The change of genes copy number plays a role in the species adaptation [18] To investigate the genetic basis potentially related to fish survival, we identified the expanded and contracted gene families in Mekong tiger perch, and 19 and 101 significantly expanded and contracted gene families were found (p-value < 0.05), separately (**Fig. 4b**). 62 contracted and 18 expanded gene families were annotated to KEGG ortholog functions. The top enriched KEGG pathway was the immune-related pathway with fifteen contracted gene families (**Fig. 4c and Supplementary table 13-14**), Furthermore, the most gene families' KO were annotated to the genes MHC1, NLRP12, ANK (ankyrin), IGH CLDN, and PLAUR (**Supplementary Table 15**), which may play a role in the adaptive immunity and survival. For example, MCH1, which was responsible for presenting peptides on the cell surface for recognition by T cells [19], was significantly contracted in *D. undecimradiatus* with only 2 copies, compared to 22 copies in closely related *L. crocea* and 14 copies in *T. rubripes* (**Fig. 4c**). NLRP12, which play a role in regulating inflammation and immunity [20], there were 13 copies in *D. undecimradiatus*, compared to 20 copies in *L. crocea and 29 copies in T. rubripes.* The contraction of immune-related genes may affect the capacity of Mekong tiger perch to adapt to environmental changes or stress, implying of human-mediated species and environmental conservation is meaningful.

Discuss

The phylogeny of Eupercaria plays a fundamental role in species classification and uncovering the species evolutionary history at the Cretaceous–Palaeogene boundary[21]. However, although species in series Eupercaria account for more than twenty percent of the bony fish, the Eupercaria phylogeny is ambiguous or conflicted, especially for the "new bush at the top". Meanwhile, the resolution of the phylogeny

bioRxiv preprint doi: https://doi.org/10.1101/787077; this version posted September 30, 2019. The copyright holder for this preprint (which was not certified by peer review) is the author/funder, who has granted bioRxiv a license to display the preprint in perpetuity. It is made available under aCC-BY-NC-ND 4.0 International license.

is currently limited to the order level, and few studies could go down to the class level or species level. Relying on limited morphological characters and molecular sequences, it is difficult to draw convincing conclusion[3-6]s. In contrast, whole genome sequencing provides sufficient information to perform the phylogenetic analysis of species. In our study, we clarified the relationship of order Lobotiformes to its related orders, Sciaenidae and Tetraodontiformes. With the rapid development of sequencing technology, large-scale fish genome sequencing projects can be achieved, such as fish 10k project (http://icg-ocean.genomics.cn/index.php/fish10kintroduction/). Those projects will greatly promote studies on the fishes' classification and evolution.

Skin color is a biologically important trait, which is a fascinating research topic and has great implications on biological adaption, commercial value, and skin health[22, 23]. In our study, most genes involved in pigmentation development, regulation and synthesis can be found in our assembled genome. However, research of underlying mechanisms is difficult to penetrate with limited genome resource. More fish genome data and molecular experiments will facilitate the analysis of skin color regulation mechanisms.

Biological conservation is an important research content of the relationship between human and nature [23], and different species vary in their adaptive capacities. In our study, immune-related genes of Mekong tiger perch were significantly contracted relative to closely related species, indicating that its environmental adaptability possibly responsible for its vulnerability. Therefore, it is necessary for humans to take various measures to protect it, such as improving the living environment, reducing fishing, artificial breeding, etc., and thus help maintain species diversity.

References

1. Roberts, T.R. and M. Kottelat, *The Indo-Pacific tiger perches: with a new species from the Mekong basin (Pisces: Coiidae)*. 1994.
2. Vidthayanon, C., *Thailand red data: fishes*. 2005.
3. Mirande, J.M., *Combined phylogeny of ray-finned fishes (Actinopterygii) and the use of*

bioRxiv preprint doi: https://doi.org/10.1101/787077; this version posted September 30, 2019. The copyright holder for this preprint (which was not certified by peer review) is the author/funder, who has granted bioRxiv a license to display the preprint in perpetuity. It is made available under aCC-BY-NC-ND 4.0 International license.

morphological characters in large-scale analyses. Cladistics, 2017. **33**(4): p. 333-350.

4. Betancur-R, R., et al., *Phylogenetic classification of bony fishes.* BMC Evolutionary Biology, 2017. **17**(1): p. 162.
5. Yang, H., et al., *Characterization of the complete mitochondrial genome sequences of three croakers (perciformes, sciaenidae) and novel insights into the phylogenetics.* International Journal of Molecular Sciences, 2018. **19**(6): p. 1741.
6. Hughes, L.C., et al., *Comprehensive phylogeny of ray-finned fishes (Actinopterygii) based on transcriptomic and genomic data.* Proceedings of the National Academy of Sciences, 2018. **115**(24): p. 6249-6254.
7. Nelson, G., *Phylogeny of major fish groups*, in *Phylogeny of major fish groups*, B. Fernholm, et al., Editors. 1989, Amsterdam: Elsevier Science. p. 325-336.
8. Protas, M.E. and N.H. Patel, *Evolution of coloration patterns.* Annual Review of Cell and Developmental Biology, 2008. **24**: p. 425-446.
9. Braasch, I., M. Schartl, and J.N. Volff, *Evolution of pigment synthesis pathways by gene and genome duplication in fish.* BMC Evolutionary Biology, 2007. **7**(1): p. 74.
10. IUCN, *The IUCN Red List of Threatened Species, version 2018-2*. 2018.
11. Wang, O., et al., *Efficient and unique cobarcoding of second-generation sequencing reads from long DNA molecules enabling cost-effective and accurate sequencing, haplotyping, and de novo assembly.* Genome Research, 2019. **29**(5): p. 798-808.
12. Weisenfeld, N.I., et al., *Direct determination of diploid genome sequences.* Genome Research, 2017. **27**(5): p. 757-767.
13. Luo, R., et al., *SOAPdenovo2: an empirically improved memory-efficient short-read de novo assembler.* Gigascience, 2012. **1**(1): p. 18.
14. Barazandeh, A., et al., *Genome-wide analysis of CpG islands in some livestock genomes and their relationship with genomic features.* Czech Journal of Animal Science, 2016. **61**(11): p. 487-495.
15. Han, L., et al., *CpG island density and its correlations with genomic features in mammalian genomes.* Genome Biology, 2008. **9**(5): p. R79.
16. Wright, S.I., N. Agrawal, and T.E. Bureau, *Effects of recombination rate and gene density on transposable element distributions in Arabidopsis thaliana.* Genome Research, 2003. **13**(8): p. 1897-1903.
17. Lorin, T., et al., *Teleost Fish-Specific Preferential Retention of Pigmentation Gene-Containing Families After Whole Genome Duplications in Vertebrates.* G3, 2018. **8**(5): p. 1795-1806.
18. Katju, V. and U. Bergthorsson, *Copy-number changes in evolution: rates, fitness effects and adaptive significance.* Front in Genetics, 2013. **4**: p. 273.
19. Wieczorek, M., et al., *Major Histocompatibility Complex (MHC) Class I and MHC Class II Proteins: Conformational Plasticity in Antigen Presentation.* Frontiers in Immunology, 2017. **8**: p. 292.
20. Tuncer, S., M.T. Fiorillo, and R. Sorrentino, *The multifaceted nature of NLRP12.* Journal of Leukocyte Biology, 2014. **96**(6): p. 991-1000.
21. Alfaro, M.E., et al., *Explosive diversification of marine fishes at the Cretaceous–Palaeogene boundary.* Nature Ecology Evolution, 2018. **2**(4): p. 688.
22. Deng, L. and S. Xu, *Adaptation of human skin color in various populations.* Hereditas, 2018. **155**(1): p. 1.

bioRxiv preprint doi: https://doi.org/10.1101/787077; this version posted September 30, 2019. The copyright holder for this preprint (which was not certified by peer review) is the author/funder, who has granted bioRxiv a license to display the preprint in perpetuity. It is made available under aCC-BY-NC-ND 4.0 International license.

297 23. Rehbein, H. and J. Oehlenschlager, *Fishery products: quality, safety and authenticity*. 2009:
298 John Wiley & Sons.

299

300

301 ## Main Tables and Figures

302 **Table 1.** Assembly and annotation of the Mekong tiger perch genome

Genome assembly		Repeat content		Genes finding and annotation	
Total Length (bp)	594,964,832	**DNA (%)**	6.11	**gene number**	29,150
Number of scaffolds	4442	**LINE (%)**	2.75	**average gene length (bp)**	13,759
longest scaffold	39.31 Mb	**SINE (%)**	0.19	**average mRNA length (bp)**	1510
N content (%)	2.17	**LTR (%)**	2.37	**average exon number per gene**	9.04
GC content	42.74	**Other (%)**	0	**average exon length (bp)**	167.03
N50 / NG50	9.73Mb / 18	**Unknown (%)**	3.35	**average intron length (bp)**	1522.83
N90 / NG90	1.41Mb / 71	**Total (%)**	11.97	**annotated genes**	19,837

303

304

305

306

307

308

309

bioRxiv preprint doi: https://doi.org/10.1101/787077; this version posted September 30, 2019. The copyright holder for this preprint (which was not certified by peer review) is the author/funder, who has granted bioRxiv a license to display the preprint in perpetuity. It is made available under aCC-BY-NC-ND 4.0 International license.

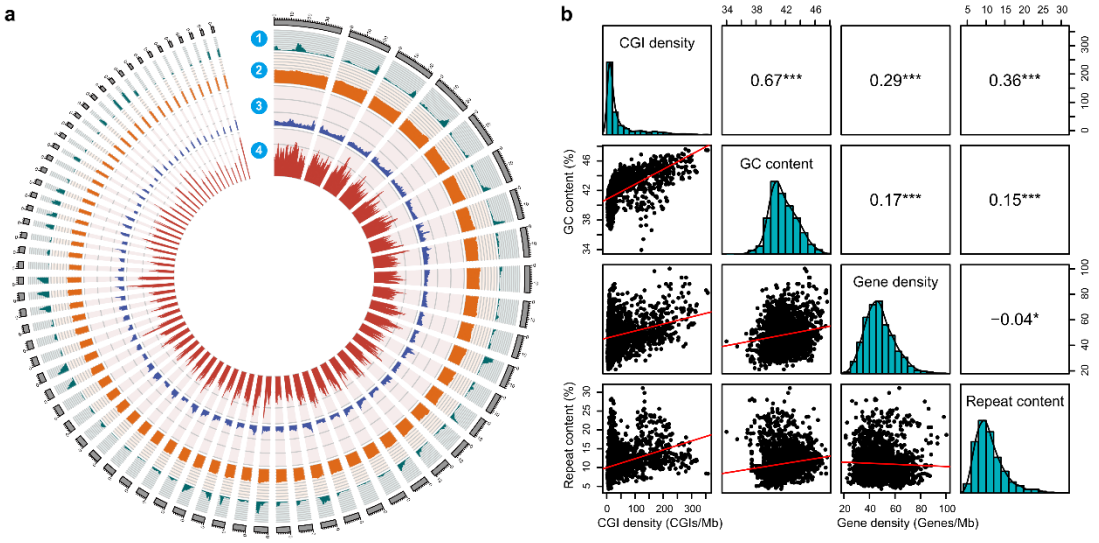

Fig1. The genome features of *D. undecimradiatus*. **(a)** A Circos plot representing four features using sliding overlapping windows of 1Mb length with 200kb step through the 71 scaffolds (scales in Mb), which accounts for 90% of genome. (1) CGI content, measured by CGIs number per million base pairs (megabase, Mb). The range of the axis is 0 to 500. (2) GC content, measured by the proportion of GC in unambiguous bases of 1 Mb window size. The range of the axis is 0 to 100. (3) Repeat content, measured by the proportion of repeat regions of 1 Mb window size. The range of the axis is 0 to 100. (4) Gene density, measured by genes number per million base pairs. **(b)** Correlation matrix plot with significance levels between four genome features. The lower triangular matrix is composed by the bivariate scatter plots with a fitted linear model. The diagonal shows the distribution by histogram with density curve. The upper triangular matrix shows the Pearson correlation plus significance level (as stars). Different significance levels are highlighted with asterisks: p-values 0.001 (***), 0.01 (**), 0.05 (*). This plot was generated with the "psych" package in R (v3.5.0).

bioRxiv preprint doi: https://doi.org/10.1101/787077; this version posted September 30, 2019. The copyright holder for this preprint (which was not certified by peer review) is the author/funder, who has granted bioRxiv a license to display the preprint in perpetuity. It is made available under aCC-BY-NC-ND 4.0 International license.

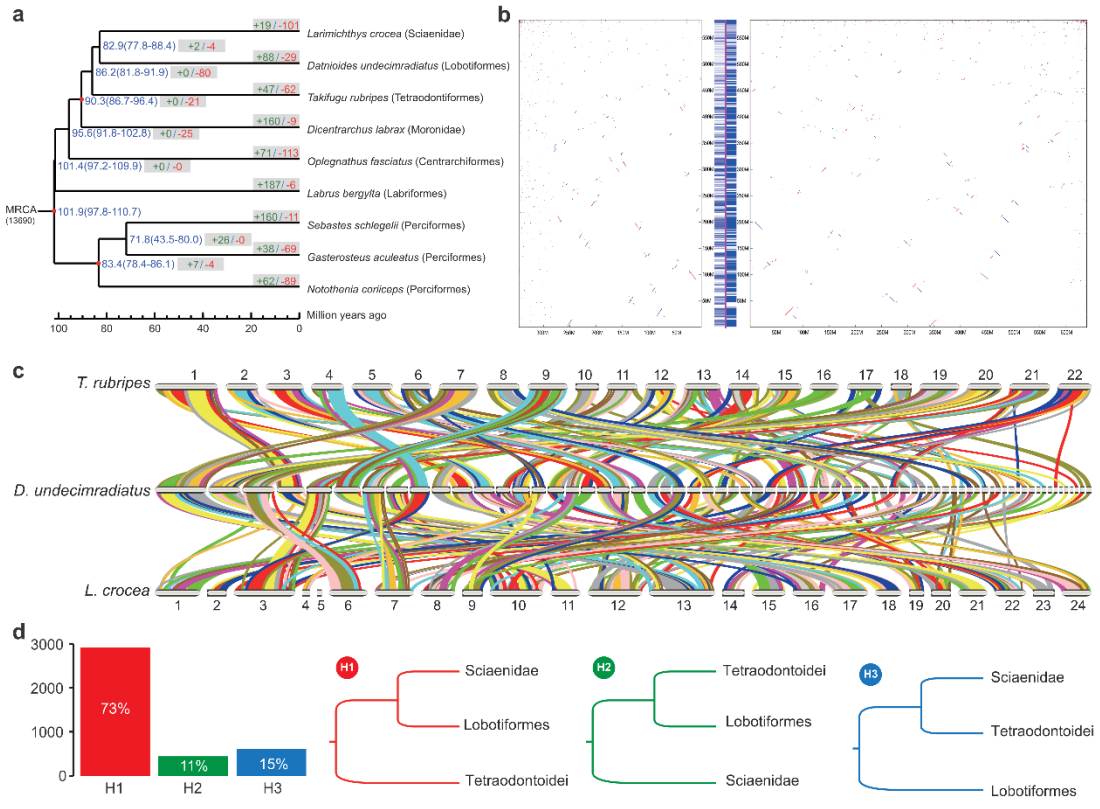

Fig. 2 The phylogenetic and genome analysis for *D. undecimradiatus* and other related species. (a) Time-calibrated maximum likelihood phylogenetic tree of nine species from Eupercaria. Red Nodes represents the calibration time points obtained from TreeTime. The estimated divergent time (mean and 95% highest-probability) are showed on the right of the nodes. Behind the divergent time, the green positive number and the red negative number in grey boxes stand for the number of gene families significantly expanded and contracted, respectively. **(b)** Synteny of *D. undecimradiatus* between *L. crocea and T. rubripes* at whole-genome nucleotide level. The y-axis represents the *D. undecimradiatus* genome, and the left x-axis refers to *T. rubripes* and right x-axis refers to *L. crocea*. The fringe plot on the left of y-axis represents the synteny regions between *D. undecimradiatus* and *T. rubripes* on *D. undecimradiatus* genome. The fringe plot on the right of y-axis represents the synteny regions between *D. undecimradiatus* and *L. crocea* on *D. undecimradiatus* genome. **(c)** synteny of *D. undecimradiatus* between *L. crocea and T. rubripes* at gene level and different colors represent different synteny blocks. **(d)** The number of gene genealogy that supports for three hypotheses concerning the Lobotiformes phylogeny.

bioRxiv preprint doi: https://doi.org/10.1101/787077; this version posted September 30, 2019. The copyright holder for this preprint (which was not certified by peer review) is the author/funder, who has granted bioRxiv a license to display the preprint in perpetuity. It is made available under aCC-BY-NC-ND 4.0 International license.

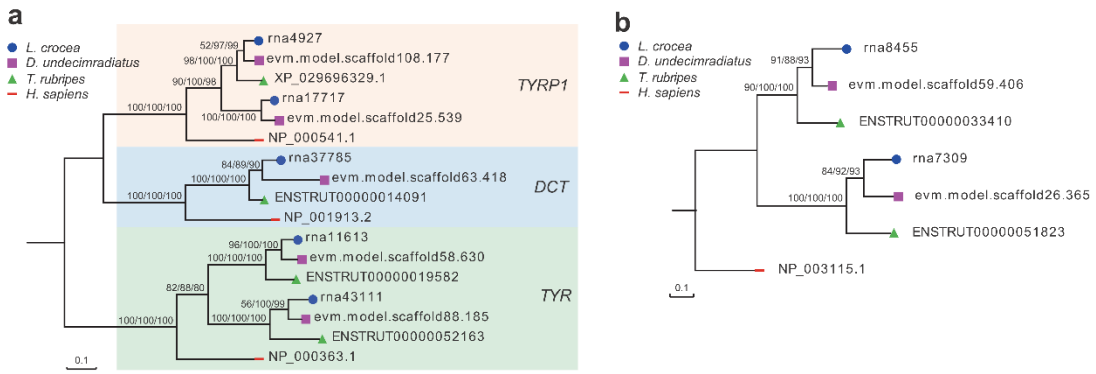

Fig. 3 The phylogeny of main rate-limiting genes involved in the pigment synthesis. (a) The concordant phylogeny of TYR gene family (*TYRP1*, *DCT* and *TYR*) using maximum likelihood, neighbor-join and minimal evolutionary methods, Corresponding bootstrap values were showed on branch labels. **(b)** The concordant phylogeny of *SPR* gene using maximum likelihood, neighbor-join and minimal evolutionary methods. Corresponding bootstrap values were showed on branch labels.

bioRxiv preprint doi: https://doi.org/10.1101/787077; this version posted September 30, 2019. The copyright holder for this preprint (which was not certified by peer review) is the author/funder, who has granted bioRxiv a license to display the preprint in perpetuity. It is made available under aCC-BY-NC-ND 4.0 International license.

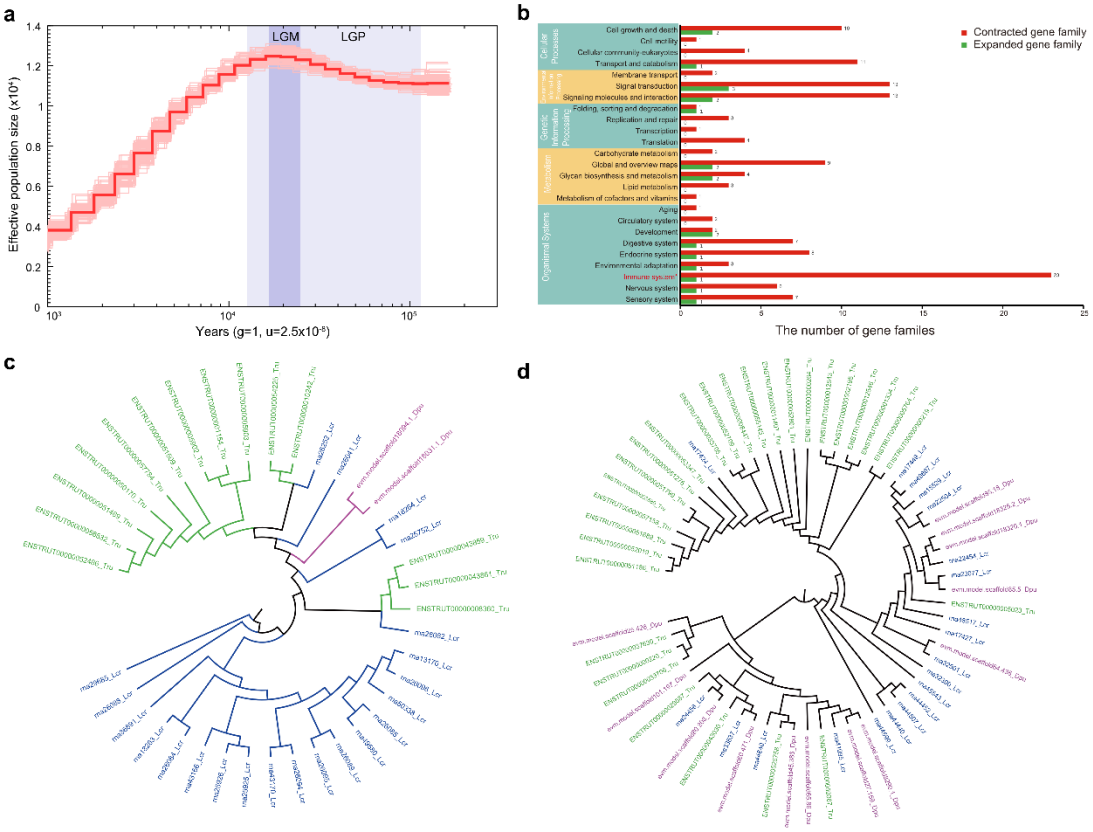

Fig. 4 The demographic history of *D. undecimradiatus* and genetic basis possibly associated with vulnerability. (a) The population history of *D. undecimradiatus* inferred using PSMC. LGM (last glacial maximum, ~26.5-19 kya) and LGP (last glacial period, ~102-1.05 kya) are shaded in gray. **(b)** The number of significantly contracted and expanded gene families (*P*-value < 0.05) involved in different KEGG pathway (at level 1 and level 2). The number at the right end of the bar indicates the number of gene families. **(c)** Phylogenetic tree of *MHC1* gene family. Green color refers to *T. rubripes*, and blue and red refers to *L. crocea* and *D. undecimradiatu* separately. **(d)** Phylogenetic tree of *NLRP12* gene family. Green color represents *T. rubripes*, and blue and red represents *L. crocea* and *D. undecimradiatu* separately.

bioRxiv preprint doi: https://doi.org/10.1101/787077; this version posted September 30, 2019. The copyright holder for this preprint (which was not certified by peer review) is the author/funder, who has granted bioRxiv a license to display the preprint in perpetuity. It is made available under aCC-BY-NC-ND 4.0 International license.

Materials and Method

DNA extraction and stLFR library construction, and sequencing

The long genomic DNA molecules were extracted from the muscle of Mekong tiger perch. The stLFR library was constructed following the standard protocol using MGIEasy stLFR library preparation kit (PN:1000005622) [11]. In details, the transposons with hybridization sequences were inserted in the long DNA molecules approximately every 200-1000 base pairs. The transposon integrated DNAs was then mixed with beads that each contained an adapter sequence. A unique barcode was shared by all adapters on each bead with a PCR primer site and a capture sequence that is complementary to the sequences on the integrated transposons. When the genomic DNA was captured to the beads, the transposons were ligated to the barcode adapters. After a few additional library-processing steps, the co-barcoded sub-fragments were sequenced on the BGISEQ-500 sequencer.

Reads filtering, genome size estimation and genome assembly

We generated a total of 1,223,801,322 million raw pair-end co-barcoding reads of 122.4 Gb. To obtain high-quality genome, SOAPnuke (v2.2) [24]was performed to filter low-quality reads (>40% low-quality bases, Q<7), PCR duplications, or adapter contaminations. After that, 753,357,182 clean pair-end reads remained. Based on the 17-mer analysis, the Mekong tiger perch genome size was estimated to be 623 Mb. Supernova assembler v 2.0.1(10X Genomics, Pleasanton, CA) were used to construct contig and scaffold, followed by gaps closing using GapCloser (v1.2) [13].

Genes structure and function annotation

We used both *de novo* approaches and homology-based approaches to predict repeat elements in *D. undecimradiatus* genome. Firstly, we aligned our genome against the Repbase database [25] at both protein and DNA levels by using RepeatMasker (v4.0.5) and RepeatProteinMasker (v4.0.5) [26] to identify transcriptional elements (TEs). Secondly, we used RepeatModeler (v1.0.8)[27] and LTR-FINDER (v1.0.6)[28] to implement *de novo* repeat annotation. Next, we used RepeatMasker to complete repeat elements identification and classification. Lastly, we combined and classified

bioRxiv preprint doi: https://doi.org/10.1101/787077; this version posted September 30, 2019. The copyright holder for this preprint (which was not certified by peer review) is the author/funder, who has granted bioRxiv a license to display the preprint in perpetuity. It is made available under aCC-BY-NC-ND 4.0 International license.

the above results. We masked the repeats in *D. undecimradiatus* genome for the subsequent gene finding.

For homology-based annotation, we downloaded protein sequences of *Dicentrarchus labrax*, *Labrus bergylta*, *Larimichthys crocea*, and *Gasterosteus aculeatus* from NCBI (https://www.ncbi.nlm.nih.gov/) and Ensembl (http://ensemblgenomes.org/). We aligned these sequence to *D. undecimradiatus* genome using BLAST[29] with an E-value cutoff of $1e^{-5}$ and the matched length coverage >30% to identify homologous genes. Based on the aligned result, we used GeneWise (v2.4.1) [30] to predict gene models. Furthermore, we used AUGUSTUS (v3.1) [31]and GENSCAN(v2009) [32] for *de novo* annotation with default parameters and zebrafish data setting as a training set of AUGUSTUS. Lastly, we integrated all above gene models by EVM [33]. We used BUSCO (v 3.0.2) [34] to assessment gene annotation integrity with three different databases, including vertebrata (v9), metazoan (v9), and vertebrata (v9).

Gene functional annotation

In order to perform gene functional annotation, we aligned above gene sets against Kyoto Encyclopedia of Genes and Genome (KEGG v87.0) [35], and NR (v84)[36] databases by blastp (E-value≤1e-5) to identify genes with similar functions. For identifying gene motifs and domains and obtaining Gene ontology (GO) terms [37], we aligned our predicted genes against ProDom [38], Pfam [39], SMART [40], PANTHER [41], and PROSITE [42] using InterProScan [43].

ncRNA annotation

Five types of ncRNA (Non-coding RNA), including tRNA, snRNA, miRNA, snRNA and, rRNA were predicted. We used tRNAscan-SE (v1.3.1) to predict tRNA in our genome with the default parameters. The genome was aligned against Rfam(v12.0) (Nawrocki E P et al., 2015) database and then we used infernal (v1.1.1) (Nawrocki E P & Eddy S R, 2013) to infer snRNA and miRNA based on mapping result. We aligned vertebrate rRNA database against *D.undecimradiatus* genome to predict rRNA.

bioRxiv preprint doi: https://doi.org/10.1101/787077; this version posted September 30, 2019. The copyright holder for this preprint (which was not certified by peer review) is the author/funder, who has granted bioRxiv a license to display the preprint in perpetuity. It is made available under aCC-BY-NC-ND 4.0 International license.

CpG islands identification

The CpG islands (CGIs), which are clusters of CpGs in CG-rich regions, were identified using CpGIScan with the parameters "--length 500 --gcc 55 --oe 0.65"[44].

Comparative genome analysis

We download the annotation files of 8 species including *Dicentrarchus labrax*, *Gasterosteus aculeatus*, *Labrus bergylta*, *Labrus bergylta*, *Notothenia coriiceps*, *Oplegnathus fasciatus*, *Larimichthys crocea*, and *Takifugu rubripes* form NCBI or Ensembl database (Suppl. Table 5). The longest transcript was extracted for each gene. We filtered error sequences that didn't have enough sequence length, with termination codon in the middle, and with sequence length not divisible by 3 to obtain raw gene sets for each species. TreeFam (v4.0) [45] was used to identify gene families.

We concatenated single-copy genes into a supergene for each species and identified fourfold degenerate sites within each supergene to construct a phylogenetic tree using RAxML (v8.2.12) [46] with GTRCATX nucleotide substitution model with parameters as "-f a -x 12345 -p 12345". Then by using the split time between *Gasterosteus aculeatus* and *Larimichthys crocea*, *Dicentrarchus labrax* and *Larimichthys crocea*, and *Notothenia coriiceps* and *Gasterosteus aculeatus* from timetree (http://www.timetree.org/) [47] as the reference time points, we estimated the divergent time between each species by MCMCtree from the PAML package with default parameters [48].

Gene family cluster and expansion and contraction analysis

Expansion and contraction of each gene family were identified by Café (v2.1) [49] based on divergence time tree. To obtain the potential functions of the gene families, the number of different KO terms was counted for each gene family. The functions of the gene families were assigned by the corresponding KO terms of more than half counts or the highest count. The KEGG pathways involved by KO terms were extracted for further functional analysis. For the phylogenetic tree of the gene family,

bioRxiv preprint doi: https://doi.org/10.1101/787077; this version posted September 30, 2019. The copyright holder for this preprint (which was not certified by peer review) is the author/funder, who has granted bioRxiv a license to display the preprint in perpetuity. It is made available under aCC-BY-NC-ND 4.0 International license.

463 the CDS sequences were fetched to construct ML tree using RAxML (v8.2.12) [46].

464

465 ***Synteny analysis***

466 The synteny analysis of *D. undecimradiatus* against *L. crocea* and *T. rubripes* was
467 performed on both whole-genome nucleotide level and gene level. On nucleotide level,
468 we used Lastz (v1.02.00) [50] to identify synteny blocks with parameters "T=2 C=2
469 H=2000 Y=3400 L=6000 K=2200", and aligned blocks less than 1 kb were filtered.

470 On gene level, we used JCVI (v0.8.12) [51] to identify synteny genes in two
471 combinations based on CDS. The JCVI carried out sequence alignment based on
472 Lastal (v979) with parameters "-u 0 -P 48 -i3G -f BlastTab". The JCVI filtered the
473 blast result based on C-score (C-score(A,B) = score(A,B) / max(best score for A, best
474 score for B)) with parameters "C-score >= 0.70 tandem_Nmax=10". We also filtered
475 out the blocks spanning less than 30 genes on the *D. undecimradiatus* genome.

476

477 ***Population demographic history inference***

478 The history of effective population size was reconstructed using PSMC (v0.6.5-r67)
479 [52]. Diploid genome reference for the individual were constructed using SAMtools
480 and BCFtools [53] with the parameters of "samtools mpileup -C30" and "vcfutils.pl
481 vcf2fq -d 10 -D 100". The demographic history was inferred using PSMC with "-N25
482 -t15 -r5 -p 4+25*2+4+6" parameters. The estimated generation time (g) and mutation
483 rate per generation per site (μ) were set to 1 and 2.5e-8.

484

485 **References**

486 24. Chen, Y., et al., *SOAPnuke: a MapReduce acceleration-supported software for integrated*
487 *quality control and preprocessing of high-throughput sequencing data.* Gigascience, 2017.
488 **7**(1): p. gix120.
489 25. Bao, W., K.K. Kojima, and O. Kohany, *Repbase Update, a database of repetitive elements in*
490 *eukaryotic genomes.* Mobile DNA, 2015. **6**(1): p. 11.
491 26. Tarailo-Graovac, M. and N. Chen, *Using RepeatMasker to identify repetitive elements in*
492 *genomic sequences.* Current protocols in bioinformatics, 2009. **25**(1): p. 4.10. 1-4.10. 14.
493 27. Smith, A. and R. Hubley. *RepeatModeler Open-1.0*. 2008; Available from:
494 http://www.repeatmasker.org.

bioRxiv preprint doi: https://doi.org/10.1101/787077; this version posted September 30, 2019. The copyright holder for this preprint (which was not certified by peer review) is the author/funder, who has granted bioRxiv a license to display the preprint in perpetuity. It is made available under aCC-BY-NC-ND 4.0 International license.

28. Xu, Z. and H. Wang, *LTR_FINDER: an efficient tool for the prediction of full-length LTR retrotransposons.* Nucleic Acids Research, 2007. **35**(Web Server issue): p. W265-8.
29. Altschul, S.F., et al., *Basic local alignment search tool.* Journal of Molecular Biology, 1990. **215**(3): p. 403-10.
30. Birney, E., M. Clamp, and R. Durbin, *GeneWise and Genomewise.* Genome Research, 2004. **14**(5): p. 988-95.
31. Stanke, M., et al., *AUGUSTUS: ab initio prediction of alternative transcripts.* Nucleic Acids Research, 2006. **34**(Web Server issue): p. W435-9.
32. Burge, C. and S. Karlin, *Prediction of complete gene structures in human genomic DNA.* Journal of Molecular Biology, 1997. **268**(1): p. 78-94.
33. Haas, B.J., et al., *Automated eukaryotic gene structure annotation using EVidenceModeler and the Program to Assemble Spliced Alignments.* Genome Biology, 2008. **9**(1): p. R7.
34. Simão, F.A., et al., *BUSCO: assessing genome assembly and annotation completeness with single-copy orthologs.* Bioinformatics, 2015. **31**(19): p. 3210-3212.
35. Kanehisa, M. and S. Goto, *KEGG: kyoto encyclopedia of genes and genomes.* Nucleic Acids Research, 2000. **28**(1): p. 27-30.
36. Pruitt, K.D., T. Tatusova, and D.R. Maglott, *NCBI reference sequences (RefSeq): a curated non-redundant sequence database of genomes, transcripts and proteins.* Nucleic Acids Research, 2007. **35**(Database issue): p. D61-5.
37. Ashburner, M., et al., *Gene ontology: tool for the unification of biology. The Gene Ontology Consortium.* Nature Genetics, 2000. **25**(1): p. 25-9.
38. Bru, C., et al., *The ProDom database of protein domain families: more emphasis on 3D.* Nucleic Acids Research, 2005. **33**(Database issue): p. D212-5.
39. Punta, M., et al., *The Pfam protein families database.* Nucleic Acids Research, 2012. **40**(Database issue): p. D290-301.
40. Ponting, C.P., et al., *SMART: identification and annotation of domains from signalling and extracellular protein sequences.* Nucleic Acids Research, 1999. **27**(1): p. 229-32.
41. Mi, H., et al., *The PANTHER database of protein families, subfamilies, functions and pathways.* Nucleic Acids Research, 2005. **33**(Database issue): p. D284-8.
42. Hulo, N., et al., *The PROSITE database.* Nucleic Acids Research, 2006. **34**(Database issue): p. D227-30.
43. Zdobnov, E.M. and R. Apweiler, *InterProScan–an integration platform for the signature-recognition methods in InterPro.* Bioinformatics
2001. **17**(9): p. 847-848.
44. Fan, Z., et al., *CpGIScan: an ultrafast tool for CpG islands identification from genome sequence.* Current Bioinformatics, 2017. **12**(2): p. 181-184.
45. Li, H., et al., *TreeFam: a curated database of phylogenetic trees of animal gene families.* Nucleic Acids Research, 2006. **34**(Database issue): p. D572-80.
46. Stamatakis, A., *RAxML version 8: a tool for phylogenetic analysis and post-analysis of large phylogenies.* Bioinformatics, 2014. **30**(9): p. 1312-3.
47. Kumar, S., et al., *TimeTree: A Resource for Timelines, Timetrees, and Divergence Times.* Molecular Biology and Evolution, 2017. **34**(7): p. 1812-1819.
48. Yang, Z., *PAML 4: phylogenetic analysis by maximum likelihood.* Molecular Biology and Evolution, 2007. **24**(8): p. 1586-91.

bioRxiv preprint doi: https://doi.org/10.1101/787077; this version posted September 30, 2019. The copyright holder for this preprint (which was not certified by peer review) is the author/funder, who has granted bioRxiv a license to display the preprint in perpetuity. It is made available under aCC-BY-NC-ND 4.0 International license.

49. Hahn, M.W., J.P. Demuth, and S.G. Han, *Accelerated rate of gene gain and loss in primates.* Genetics, 2007. **177**(3): p. 1941-9.
50. Harris, R.S., *Improved pairwise Alignmnet of genomic DNA.* 2007.
51. Tang, H., et al., *jcvi: JCVI utility libraries.* Zenodo, 2015: p. 10.5281/zenodo.31631.
52. Li, H. and R. Durbin, *Inference of human population history from individual whole-genome sequences.* Nature, 2011. **475**(7357): p. 493-6.
53. Li, H., et al., *The Sequence Alignment/Map format and SAMtools.* Bioinformatics, 2009. **25**(16): p. 2078-9.

Data available

The sequencing reads of Mekong tiger perch in this study have been deposited in NCBI Sequence Read Archive (SRA) under BioProject accession PRJNA574247. The datasets reported in this study are also available in the CNGB under accession number CNP0000691.

Acknowledgements

This work was financially supported by the special funding of “Blue granary” scientific and technological innovation of China (2018YFD0900301-05) and Special Fund for Marine Economic Development of Fujian Province (ZHHY-2019-3). We also thanks for the technical support of stLFR library construction and sequencing from China National Genebank.

Author Contributions

X. L., G. F. and H. Z. conceived the project. S. L. and G. F. supervised the study. M. Z. contributed to sample collections. S. S., Y. W., L. L., and X. H. performed bioinformatics analyses. S. S, Y.W., G. F., X. L., and X. D. wrote the manuscript with help from all co-authors.

Competing Interests

The authors declare no competing interests.

bioRxiv preprint doi: https://doi.org/10.1101/787077; this version posted September 30, 2019. The copyright holder for this preprint (which was not certified by peer review) is the author/funder, who has granted bioRxiv a license to display the preprint in perpetuity. It is made available under aCC-BY-NC-ND 4.0 International license.

Supplementary Figures and Tables

Supplementary figure 1. The photo of the Mekong tiger perch captured in Mekong river.

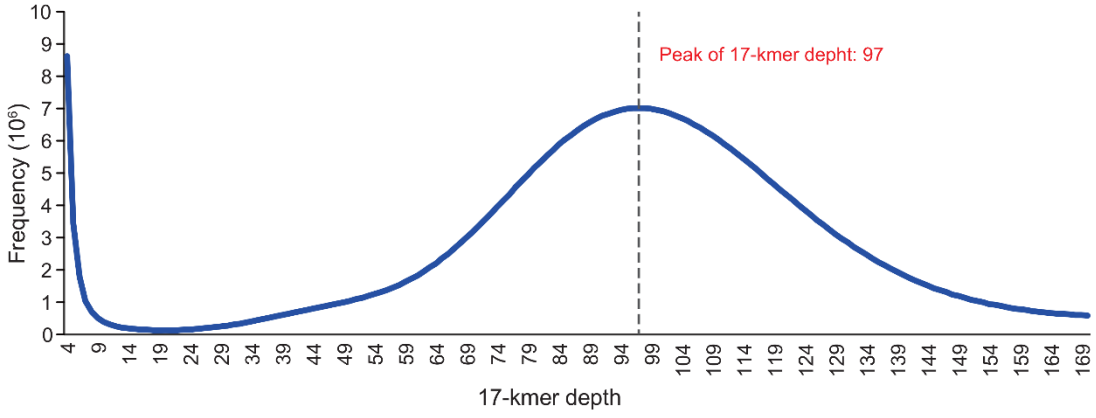

Supplementary figure 2. Kmer (K=17) frequency at different Kmer depth. The total number of Kmer is 60,437,782,622, the Kmer depth peak at 97, and the reads sequencing length was 100, so that the genome size was estimated 623,069,923bp.

bioRxiv preprint doi: https://doi.org/10.1101/787077; this version posted September 30, 2019. The copyright holder for this preprint (which was not certified by peer review) is the author/funder, who has granted bioRxiv a license to display the preprint in perpetuity. It is made available under aCC-BY-NC-ND 4.0 International license.

585 **Supplementary table 1.** The details of longest 71 scaffolds.

scaffold ID	Length (bp)	GC content (%)	N_ratio (%)
scaffold22	39,306,008	42.33	1.58
scaffold23	24,901,081	42.33	1.97
scaffold24	23,317,972	42.03	0.87
scaffold63	22,660,142	42.41	1.76
scaffold26	19,767,337	41.45	0.89
scaffold27	19,537,586	42.15	1.03
scaffold58	17,534,777	41.68	2.25
scaffold25	17,129,097	41.35	2.02
scaffold28	15,606,803	41.60	0.76
scaffold45	15,041,297	41.93	1.28
scaffold60	13,384,554	42.11	0.81
scaffold61	13,186,598	42.71	1.04
scaffold77	11,679,837	42.19	2.24
scaffold79	11,352,832	42.26	0.96
scaffold59	10,986,376	41.77	1.75
scaffold88	10,659,222	41.96	1.16
scaffold89	9,983,168	43.64	3.77
scaffold62	9,730,178	42.24	1.24
scaffold64	9,455,329	41.09	0.99
scaffold80	9,009,409	41.98	1.13
scaffold90	8,890,068	44.17	5.80
scaffold66	7,986,709	42.51	0.72
scaffold67	7,981,977	42.51	0.72
scaffold155	7,882,590	44.18	2.10
scaffold76	7,221,551	42.34	0.79
scaffold83	7,024,340	43.41	1.36
scaffold129	7,004,772	43.25	3.18
scaffold86	6,951,544	44.19	2.53
scaffold87	6,939,792	42.63	1.33
scaffold85	6,732,700	43.19	2.76
scaffold75	6,668,441	40.74	0.60
scaffold102	6,529,773	42.51	1.49
scaffold78	6,505,070	40.03	1.04
scaffold110	6,218,238	42.57	2.73
scaffold65	6,149,668	41.30	0.92
scaffold81	6,042,282	40.32	0.84
scaffold107	5,552,807	43.61	1.57
scaffold82	5,383,449	45.41	3.42
scaffold108	5,037,774	42.28	1.01
scaffold111	4,837,472	43.64	1.99
scaffold105	4,507,353	42.91	1.23
scaffold101	4,379,686	46.21	5.84

bioRxiv preprint doi: https://doi.org/10.1101/787077; this version posted September 30, 2019. The copyright holder for this preprint (which was not certified by peer review) is the author/funder, who has granted bioRxiv a license to display the preprint in perpetuity. It is made available under aCC-BY-NC-ND 4.0 International license.

scaffold176	4,245,196	46.52	3.11
scaffold125	4,183,443	46.18	1.54
scaffold84	3,961,987	40.27	0.99
scaffold106	3,649,163	43.70	1.26
scaffold148	3,238,164	41.03	2.37
scaffold147	3,070,712	47.24	2.74
scaffold103	2,911,789	45.84	9.75
scaffold69	2,816,955	45.17	5.65
scaffold68	2,814,068	45.16	5.64
scaffold131	2,714,138	42.91	2.44
scaffold186	2,711,499	39.58	0.54
scaffold200	2,366,470	46.18	4.82
scaffold113	2,352,837	42.56	3.55
scaffold104	2,165,782	41.93	0.79
scaffold201	2,162,358	43.22	0.86
scaffold122	2,118,146	46.78	8.16
scaffold133	2,111,711	41.92	4.03
scaffold18494	1,965,245	45.72	4.53
scaffold18500	1,963,021	45.71	4.53
scaffold124	1,863,279	46.42	5.63
scaffold112	1,679,604	41.45	0.25
scaffold109	1,675,575	42.10	2.24
scaffold137	1,624,607	42.65	3.82
scaffold173	1,554,608	43.17	0.68
scaffold130	1,511,149	41.63	2.51
scaffold185	1,502,512	43.66	3.3
scaffold136	1,485,443	43.24	2.61
scaffold127	1,411,413	46.76	6.74
scaffold135	1,407,639	47.20	6.86

586

Supplementary table 2. Repeat annotation of the Mekong tiger perch genome.

Type	Repbase TEs		TE proteins		De novo		Combined TEs	
	Length (bp)	% in genome	Length (bp)	% in genome	Length (bp)	% in genome	Length (bp)	% in genome
DNA	16,506,661	2.77	1,633,161	0.27	30,824,896	5.18	36,324,964	6.11
LINE	6,821,950	1.15	4,071,954	0.68	12,961,236	2.18	16,349,136	2.75
SINE	662,765	0.11	-	0.00	908,953	0.15	1,152,466	0.19
LTR	6,332,971	1.06	1,837,976	0.31	9,602,730	1.61	14,084,966	2.37
Other	4,319	0.00	-	0.00	-	0.00	4,319	0.00
Unknown	-	0.00	-	0.00	19,939,915	3.35	19,939,915	3.35
Total	26,352,522	4.43	7,536,991	1.27	65,356,559	10.98	71,231,464	11.97

Supplementary table 3. The statistics of predicted genes using different methods.

Method	Software/Species	Number of predicted genes	Average gene length (bp)	Average CDS length (bp)	Average exon number	Average exon length (bp)	Average intron length (bp)
ab initio	Augustus	26,826	11324.91	1428.76	8.21	173.94	1371.75
	Genscan	29,524	14516.5	1596.21	9.18	173.87	1579.41
Homolog-based	*Danio rerio*	44,300	19786.39	1526.41	8.79	173.62	2343.59
	Dicentrarchus labrax	28,264	12505.75	1483.79	8.13	182.44	1545.24
	Labrus bergylta	39,412	21851.38	1494.87	8.67	172.36	2653.06
	Larimichthys crocea	47,139	19654.28	2187.95	12.62	173.42	1503.63
	Gasterosteus aculeatus	28,975	10277.3	1456.49	8.92	163.2	1113.07
Combined	EVM	29,150	13758.59	1510.42	9.04	167.03	1522.83

bioRxiv preprint doi: https://doi.org/10.1101/787077; this version posted September 30, 2019. The copyright holder for this preprint (which was not certified by peer review) is the author/funder, who has granted bioRxiv a license to display the preprint in perpetuity. It is made available under aCC-BY-NC-ND 4.0 International license.

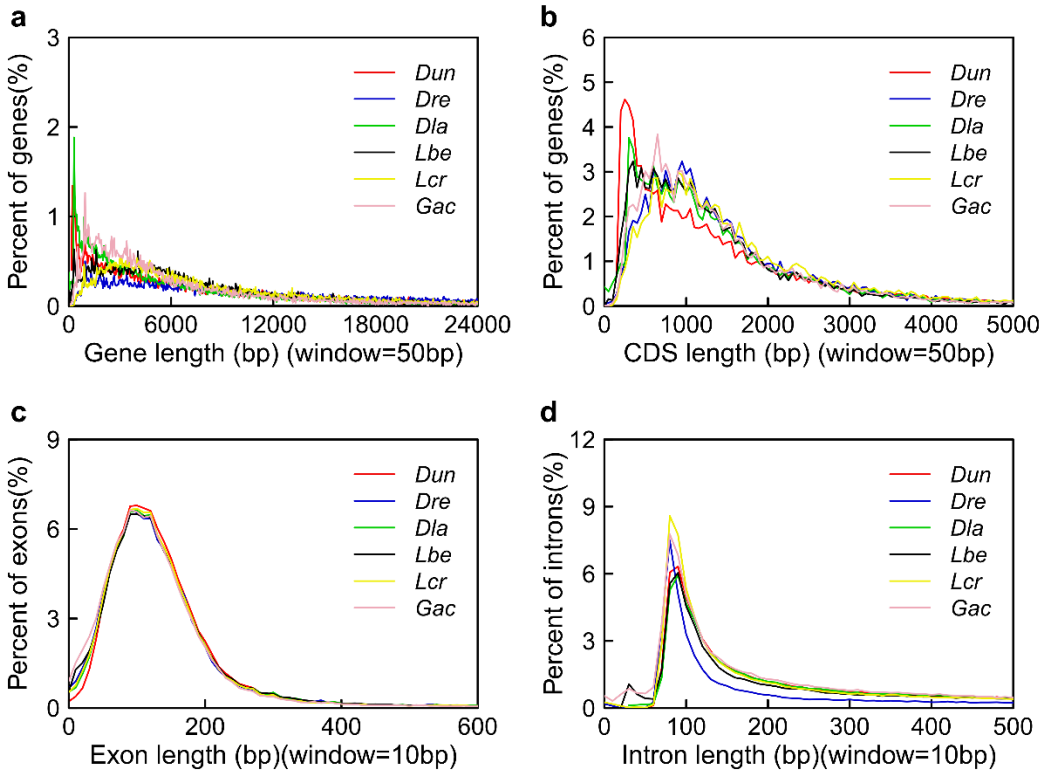

590

591 **Supplementary figure 3.** The distribution of gene length, CDS length, exon length
592 and intron length of the Mekong tiger perch compared to related speices. Scientific
593 names are abbreviated as follows: ***Dun***, *Datnioides undecimradiatus*; ***Dre***, *Danio*
594 *rerio*; ***Dla***, *Dicentrarchus labrax*; ***Lbe***, *Labrus bergylta*; ***Lcr***, *Larimichthys crocea*;
595 ***Gac***, *Gasterosteus aculeatus.*

596

597 **Supplementary table 4.** ncRNA annotation of the Mekong tiger perch genome.

Type	Sub-type	Copy number	Average length (bp)	Total length (bp)	% of genome
miRNA	-	260	82.73	21509	0.003615
tRNA	-	753	76.03	57248	0.009622
rRNA	rRNA	98	184.79	18109	0.003044
	18S	12	388.33	4660	0.000783
	28S	47	215.021	10106	0.001699
	5.8S	7	117.14	820	0.000138
	5S	32	78.84	2523	0.000424
snRNA	snRNA	261	126.20	32938	0.005536
	CD-box	117	94.60	11068	0.001860
	HACA-box	77	154.45	11893	0.001999
	splicing	58	140.03	8122	0.001365

bioRxiv preprint doi: https://doi.org/10.1101/787077; this version posted September 30, 2019. The copyright holder for this preprint (which was not certified by peer review) is the author/funder, who has granted bioRxiv a license to display the preprint in perpetuity. It is made available under aCC-BY-NC-ND 4.0 International license.

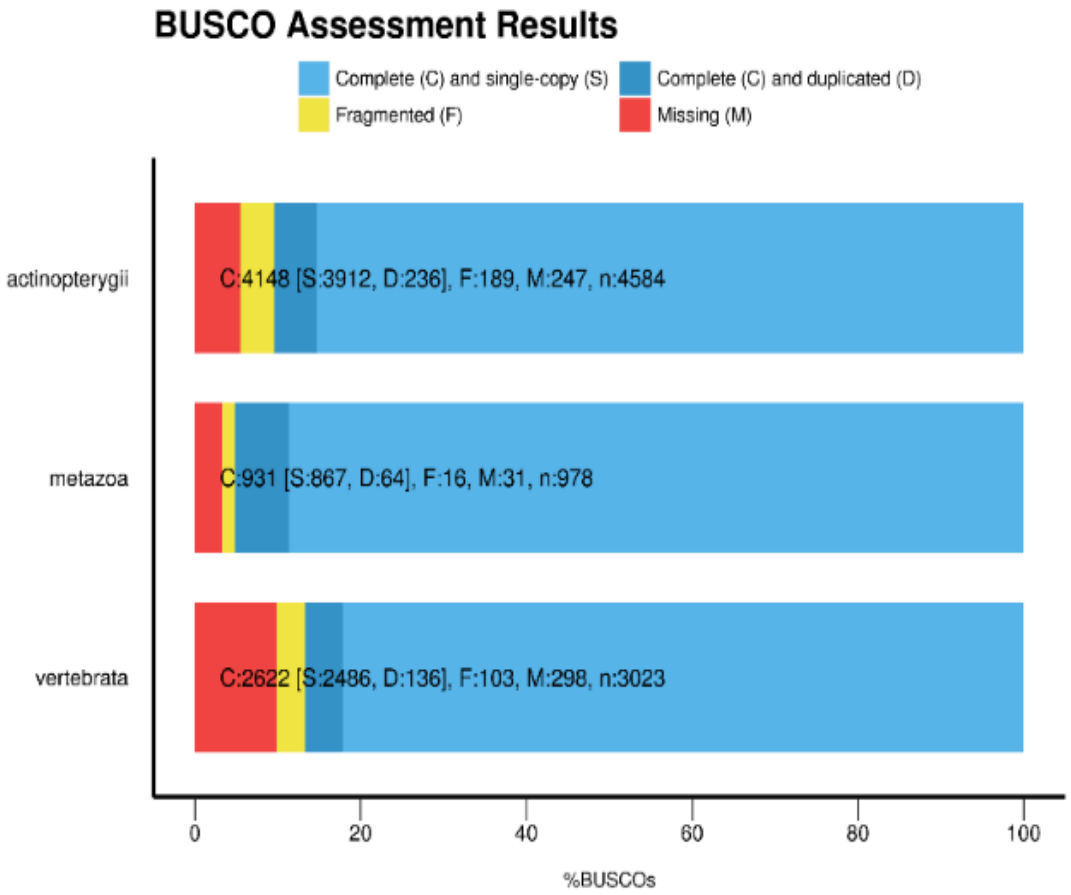

598

599 **Supplementary figure 4.** The completeness of predicted genes sets was evaluated by
600 BUSCO based on three different databases, including Actinopterygii (v9), metazoan
601 (v9) and vertebrata (v9).

Supplementary table 5. Genes annotated on mitochondrial genome.

Mitochondrial genome	Start	End	Length(bp)	Direction	Type	Gene name	Gene product	Occurred Counts
C515351	134	202	69	+	tRNA	trnF(gaa)	tRNA-Phe	1
C515351	202	1170	969	+	rRNA	s-rRNA	12S ribosomal RNA	1
C515351	1170	1242	73	+	tRNA	trnV(uac)	tRNA-Val	1
C515351	1262	2954	1693	+	rRNA	l-rRNA	16S ribosomal RNA	1
C515351	2954	3028	75	+	tRNA	trnL(uaa)	tRNA-Leu	2
C515351	3028	4003	976	+	CDS	ND1	NADH dehydrogenase subunit 1	1
C515351	4008	4079	72	+	tRNA	trnI(gau)	tRNA-Ile	1
C515351	4078	4149	72	-	tRNA	trnQ(uug)	tRNA-Gln	1
C515351	4148	4220	73	+	tRNA	trnM(cau)	tRNA-Met	1
C515351	4220	5267	1048	+	CDS	ND2	NADH dehydrogenase subunit 2	1
C515351	5266	5338	73	+	tRNA	trnW(uca)	tRNA-Trp	1
C515351	5338	5407	70	-	tRNA	trnA(ugc)	tRNA-Ala	1
C515351	5408	5481	74	-	tRNA	trnN(guu)	tRNA-Asn	1
C515351	5516	5585	70	-	tRNA	trnC(gca)	tRNA-Cys	1
C515351	5585	5655	71	-	tRNA	trnY(gua)	tRNA-Tyr	1
C515351	5656	7207	1552	+	CDS	COX1	cytochrome c oxidase subunit I	1
C515351	7207	7278	72	-	tRNA	trnS(uga)	tRNA-Ser	2
C515351	7281	7354	74	+	tRNA	trnD(guc)	tRNA-Asp	1
C515351	7362	8061	700	+	CDS	COX2	cytochrome c oxidase subunit II	1
C515351	8053	8128	76	+	tRNA	trnK(uuu)	tRNA-Lys	1

C515351	8129	8297	169	+	CDS	ATP8	ATP synthase F0 subunit 8	1
C515351	8314	8971	658	+	CDS	ATP6	ATP synthase F0 subunit 6	1
C515351	8970	9756	787	+	CDS	COX3	cytochrome c oxidase subunit III	1
C515351	9755	9827	73	+	tRNA	trnG(ucc)	tRNA-Gly	1
C515351	9827	10178	352	+	CDS	ND3	NADH dehydrogenase subunit 3	1
C515351	10176	10245	70	+	tRNA	trnR(ucg)	tRNA-Arg	1
C515351	10245	10542	298	+	CDS	ND4L	NADH dehydrogenase 4L	1
C515351	10535	11921	1387	+	CDS	ND4	NADH dehydrogenase 4	1
C515351	11916	11984	69	+	tRNA	trnH(gug)	tRNA-His	1
C515351	11984	12051	68	+	tRNA	trnS(gcu)	tRNA-Ser	2
C515351	12055	12128	74	+	tRNA	trnL(uag)	tRNA-Leu	2
C515351	12128	13967	1840	+	CDS	ND5	NADH dehydrogenase subunit 5	1
C515351	13963	14485	523	-	CDS	ND6	NADH dehydrogenase 6	1
C515351	14486	14555	70	-	tRNA	trnE(uuc)	tRNA-Glu	1
C515351	14560	15721	1162	+	CDS	CYTB	cytochrome b	1
C515351	15701	15771	71	+	tRNA	trnT(ugu)	tRNA-Thr	1
C515351	15770	15840	71	-	tRNA	trnP(ugg)	tRNA-Pro	1

Supplementary table 6. Relationship GC with repeat content.

Pairs	Pearson r	Lower 95% CI	Upper 95% CI	*P*-value
CGI density vs. GC content	0.643	0.666	0.688	4.83E-304
CGI density vs. Gene density	0.252	0.290	0.326	4.37E-47
CGI density vs. Repeat content	0.329	0.364	0.399	1.75E-75
GC content vs. Gene density	0.135	0.174	0.213	1.42E-17
GC content vs. Repeat content	0.108	0.147	0.187	5.27E-13
Gene density vs. Repeat content	-0.082	-0.042	-0.002	4.16E-02

Supplementary table 7. Nine species used in our study.

Three letter code	Scientific name	Common name	Order	Data source	Accession ID
Ofa	*Oplegnathus fasciatus*	barred knifejaw	Centrarchiformes	NCBI	GCA_003416845.1
Lbe	*Labrus bergylta*	ballan wrasse	Labriformes	NCBI	GCF_900080235.1
Dun	*Datnioides undecimradiatus*	Mekong tiger perch	Lobotiformes	our study	our study
Dla	*Dicentrarchus labrax*	European seabass	Moronidae	NCBI	GCA_000689215.1
Gac	*Gasterosteus aculeatus*	three-spined stickleback	Perciformes	NCBI	GCA_000180675.1
Nco	*Notothenia coriiceps*	black rockcod	Perciformes	NCBI	GCF_000735185.1
Ssc	*Sebastes schlegelii*	Schlegel's black rockfish	Perciformes	NCBI	GCA_004335315.1
Lcr	*Larimichthys crocea*	large yellow croaker	Sciaenidae	NCBI	GCF_000972845.2
Tru	*Takifugu rubripes*	torafugu	Tetraodontiformes	NCBI	GCF_000180615.1

bioRxiv preprint doi: https://doi.org/10.1101/787077; this version posted September 30, 2019. The copyright holder for this preprint (which was not certified by peer review) is the author/funder, who has granted bioRxiv a license to display the preprint in perpetuity. It is made available under aCC-BY-NC-ND 4.0 International license.

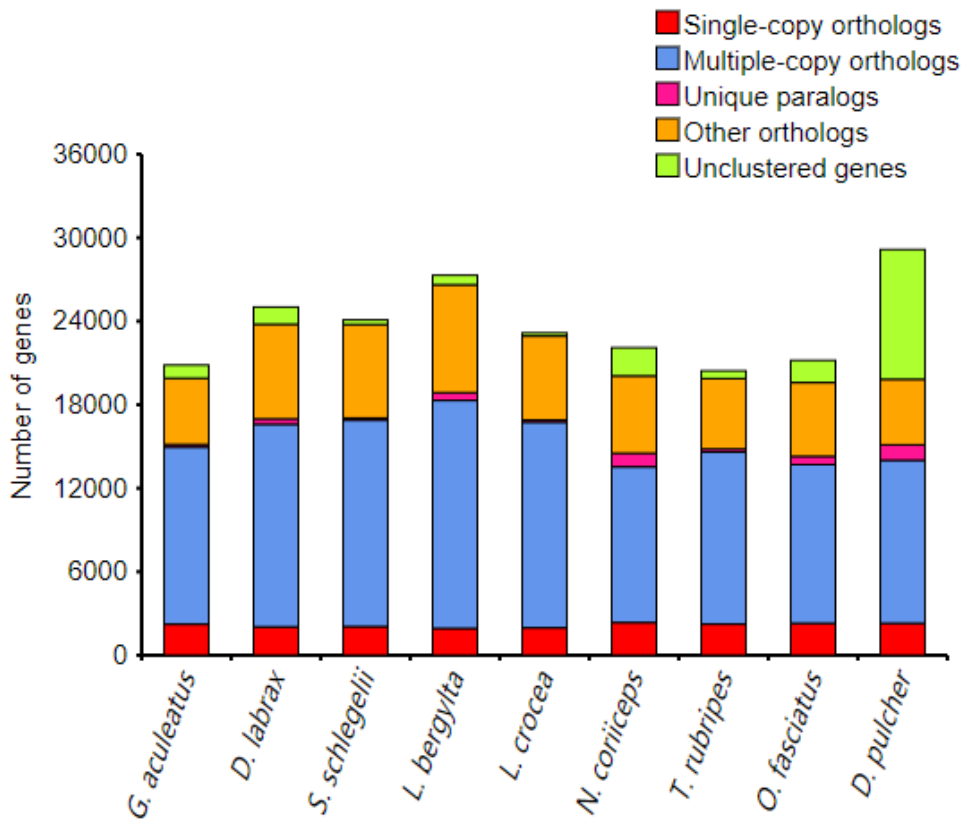

Supplementary figure 5. The genes number of five type of gene families for nine species used in the analysis of comparative genomes.

Supplementary table 8. The statistics of gene family clusters.

Species	Genes* number	Un-clustered genes number	Families number	Unique family's number	Average genes per family
Gac	20,862	1,107	8,792	19	2.25
Dla	25,020	1,423	10,090	77	2.34
Ssc	24,094	425	9,745	21	2.43
Lbe	27,305	888	10,031	133	2.63
Lcr	23,163	315	9,967	30	2.29
Nco	22,099	2,713	9,752	139	1.99
Tru	20,434	704	9,359	37	2.11
Ofa	21,901	2,023	9,481	81	2.10
Dun	26,894	8,260	9,208	378	2.02

* Pseudo-genes (stop-gained in middle) were filtered out, and the genes with protein length <50 were also removed.

bioRxiv preprint doi: https://doi.org/10.1101/787077; this version posted September 30, 2019. The copyright holder for this preprint (which was not certified by peer review) is the author/funder, who has granted bioRxiv a license to display the preprint in perpetuity. It is made available under aCC-BY-NC-ND 4.0 International license.

617 **Supplementary table 9.** Synteny of alignment statistics at whole-genome nucleotide
618 sequences level.

Species aligned to *Dun*	Cutoff of alignment length	Synteny coverage (%)	Alignment number	Average alignment length (bp)	Median alignment length (bp)	Min alignment length (bp)	Max alignment length (bp)
Lcr	≥ 1kb	41.13%	105,447	2,321	1,717	1,000	56,540
(length:658	≥ 2kb	26.02%	41,422	3,738	2,967	2,000	56,540
M)	≥ 5kb	8.89%	6,811	7,769	6,571	5,000	56,540
Tru	≥ 1kb	10.04%	36,032	1,657	1,388	1,000	24,987
(length:391	≥ 2kb	3.58%	7,312	2,552	2,954	2,000	24,987
M)	≥ 5kb	0.39%	352	6,621	5,952	5,000	24,987

619
620 **Supplementary table 10.** Distribution of synteny of alignment statistics at whole
621 genes level at different cutoff.

Species aligned to *Dun*	Cutoff of block length*	Synteny coverage (%)	Block number	Average block length	Median block length	Min block length	Max block length
Lcr	>= 4	91.24	529	50.28	28	4	679
(gene	>= 10	89.19	433	60.05	34	10	679
number:		77.92	255	89.07	58	30	679
23423)	>= 30						
Tru	>= 4	83.97	593	41.28	20	4	542
(gene	>= 10	80.93	452	52.19	29	10	542
number:		66.95	222	87.91	54	30	542
28679)	>= 30						

622 * block length was defined as the spanning genes number on *Dun*.
623

Supplementary table 11. Genome assembly and gene set quality by BUSCO.

		Genome level		Gene level	
		Larimichthys crocea	*Takifugu rubripes*	*Larimichthys crocea*	*Takifugu rubripes*
actinopterygii (db_v9)	Complete BUSCOs (C)	4362 (95.2%)	4263 (93.0%)	4554 (99.3%)	4345 (94.7%)
	Complete and single-copy BUSCOs (S)	4275 (93.3%)	4168 (90.9%)	2615 (57.0%)	3000 (65.4%)
	Complete and duplicated BUSCOs (D)	87 (1.9%)	95 (2.1%)	1939 (42.3%)	1345 (29.3%)
	Fragmented BUSCOs (F)	119 (2.6%)	202 (4.4%)	23 (0.5%)	134 (2.9%)
	Missing BUSCOs (M)	103 (2.2%)	119 (2.6%)	7 (0.2%)	105 (2.4%)
	Total BUSCO groups searched	4584	4584	4584	4584
metazoa (db_v9)	Complete BUSCOs (C)	918 (93.9%)	915 (93.6%)	973 (99.5%)	950 (97.1%)
	Complete and single-copy BUSCOs (S)	882 (90.2%)	880 (90.0%)	656 (67.1%)	670 (68.5%)
	Complete and duplicated BUSCOs (D)	36 (3.7%)	35 (3.6%)	317 (32.4%)	280 (28.6%)
	Fragmented BUSCOs (F)	7 (0.7%)	12 (1.2%)	4 (0.4%)	15 (1.5%)
	Missing BUSCOs (M)	53 (5.4%)	51 (5.2%)	1 (0.1%)	13 (1.4%)
	Total BUSCO groups searched	978	978	978	978

bioRxiv preprint doi: https://doi.org/10.1101/787077; this version posted September 30, 2019. The copyright holder for this preprint (which was not certified by peer review) is the author/funder, who has granted bioRxiv a license to display the preprint in perpetuity. It is made available under aCC-BY-NC-ND 4.0 International license.

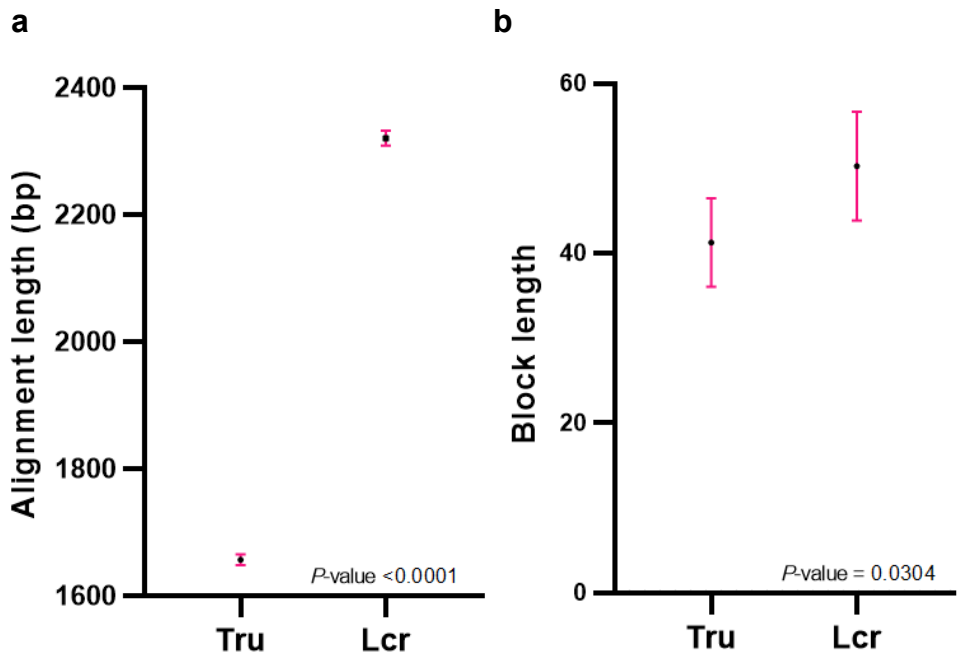

Supplementary figure 6. The t-test statistics of alignment length and block length. **(a)** The distribution of the length of synteny blocks at nucleotide-level. *P*-value was calculated using t-statistic. **(b)** The distribution of the length of synteny blocks at gene-level. *P*-value was using t-statistic.

Supplementary table 12. Genes involved in the pigment synthesis.

Pigmentary_function	Gene	Gene ID
Components of melanosomes	gpnmb	evm.model.scaffold89.24
Components of melanosomes	slc24a4	evm.model.scaffold22.131;
Components of melanosomes	trpm1	evm.model.scaffold27.487;
Components of melanosomes	tspan10	evm.model.scaffold80.229;
Components of melanosomes	vat1	evm.model.scaffold18344.71;evm.model.scaffold18367.69;evm.model.scaffold60.236
Iridophores	chm	evm.model.scaffold200.145
Iridophores	csf1	evm.model.scaffold64.448
Iridophores	ece2	evm.model.scaffold75.239
Iridophores	fbxw4	evm.model.scaffold111.35;
Iridophores	fhl2	evm.model.scaffold61.509;evm.model.scaffold63.296;evm.model.scaffold82.226
Iridophores	foxd3	evm.model.scaffold23.901;
Iridophores	gart	evm.model.scaffold82.268;

bioRxiv preprint doi: https://doi.org/10.1101/787077; this version posted September 30, 2019. The copyright holder for this preprint (which was not certified by peer review) is the author/funder, who has granted bioRxiv a license to display the preprint in perpetuity. It is made available under aCC-BY-NC-ND 4.0 International license.

Iridophores	ltk	evm.model.scaffold61.336;
Iridophores	med12	evm.model.scaffold81.240;
Iridophores	mpv17	evm.model.scaffold18251.25;evm.model.scaffold18349.23;
Iridophores	trim33	evm.model.scaffold158.1;
Iridophores, Melanocyte development	ednrb	evm.model.scaffold76.195;evm.model.scaffold62.302;evm.model.scaffold63.409;
Iridophores, Melanocyte development	impdh1	evm.model.scaffold27.353;evm.model.scaffold66.197;evm.model.scaffold67.196;
Iridophores, Melanocyte development	oca2	evm.model.scaffold23.184
Iridophores, Melanocyte development	sox9	evm.model.scaffold80.182;
Iridophores, Melanocyte development, Xanthophore differentiation	sox10	evm.model.scaffold85.272;
Leucophores, Pteridine synthesis	xdh	evm.model.scaffold82.33;
Leucophores, Xanthophore differentiation	gch1	evm.model.scaffold110.30;
Leucophores, Xanthophore differentiation	pax7	evm.model.scaffold24.275;
Leucophores, Xanthophore differentiation	slc2a11	evm.model.scaffold60.596;evm.model.scaffold24.381;evm.model.scaffold24.795;evm.model.scaffold26.142
Melanocyte development	adam17	evm.model.scaffold61.347;
Melanocyte development	adamts20	evm.model.scaffold27.709;
Melanocyte development	adrb2	evm.model.scaffold62.231;
Melanocyte development	apc	evm.model.scaffold155.410;
Melanocyte development	atp6v0b	evm.model.scaffold75.6;
Melanocyte development	bcl2	evm.model.scaffold75.147;
Melanocyte development	brsk2	evm.model.scaffold27.208;evm.model.scaffold89.353
Melanocyte development	c10orf11	evm.model.scaffold28.337;evm.model.scaffold28.342
Melanocyte development	cited1	evm.model.scaffold157.20
Melanocyte development	creb1	evm.model.scaffold63.159;
Melanocyte development	dct	evm.model.scaffold63.418;
Melanocyte development	dock7	evm.model.scaffold23.909;evm.model.scaffold80.316
Melanocyte development	eda	evm.model.scaffold62.157
Melanocyte development	edar	evm.model.scaffold63.630;
Melanocyte development	edn3	evm.model.scaffold24.1046;evm.model.scaffold64.123;

bioRxiv preprint doi: https://doi.org/10.1101/787077; this version posted September 30, 2019. The copyright holder for this preprint (which was not certified by peer review) is the author/funder, who has granted bioRxiv a license to display the preprint in perpetuity. It is made available under aCC-BY-NC-ND 4.0 International license.

Melanocyte development	ednrb2	evm.model.scaffold173.15;evm.model.scaffold90.41
Melanocyte development	egfr	evm.model.scaffold75.24;
Melanocyte development	en1	evm.model.scaffold83.123
Melanocyte development	erbb3	evm.model.scaffold24.541;
Melanocyte development	fgfr2	evm.model.scaffold28.677;
Melanocyte development	frem2	evm.model.scaffold25.244;evm.model.scaffold58.224;evm.model.scaffold88.161
Melanocyte development	fzd4	evm.model.scaffold58.625;
Melanocyte development	gata3	evm.model.scaffold17418.1;
Melanocyte development	gfpt1	evm.model.scaffold176.182;
Melanocyte development	gja5	evm.model.scaffold63.370;
Melanocyte development	gli3	evm.model.scaffold45.346;
Melanocyte development	gnaq	evm.model.scaffold26.243;
Melanocyte development	gpc3	evm.model.scaffold62.322;evm.model.scaffold62.324;
Melanocyte development	gpr161	evm.model.scaffold63.326;
Melanocyte development	hdac1	evm.model.scaffold87.53;
Melanocyte development	hps1	evm.model.scaffold28.431;
Melanocyte development	hps4	evm.model.scaffold176.213;
Melanocyte development	hps6	evm.model.scaffold28.443;
Melanocyte development	hsd3b1	evm.model.scaffold121.40
Melanocyte development	igsf11	evm.model.scaffold88.256
Melanocyte development	ikbkg	evm.model.scaffold153.7;
Melanocyte development	irf4	evm.model.scaffold23.1068;
Melanocyte development	itgb1	evm.model.scaffold107.36;evm.model.scaffold45.427
Melanocyte development	kcnj13	evm.model.scaffold148.100
Melanocyte development	kit	evm.model.scaffold23.254;
Melanocyte development	kitlg	evm.model.scaffold27.925
Melanocyte development	lmx1a	evm.model.scaffold23.711;evm.model.scaffold80.296
Melanocyte development	mbtps1	evm.model.scaffold105.8;
Melanocyte development	mcoln3	evm.model.scaffold107.276;evm.model.scaffold23.933
Melanocyte development	mef2c	evm.model.scaffold26.63;
Melanocyte development	mib1	evm.model.scaffold75.31;
Melanocyte development	mib2	evm.model.scaffold130.11;
Melanocyte development	mitf	evm.model.scaffold24.917;evm.model.scaffold90.355
Melanocyte development	mreg	evm.model.scaffold63.744
Melanocyte development	myc	evm.model.scaffold45.322;
Melanocyte development	myo5a	evm.model.scaffold89.43;
Melanocyte development	oprm1	evm.model.scaffold28.210;

bioRxiv preprint doi: https://doi.org/10.1101/787077; this version posted September 30, 2019. The copyright holder for this preprint (which was not certified by peer review) is the author/funder, who has granted bioRxiv a license to display the preprint in perpetuity. It is made available under aCC-BY-NC-ND 4.0 International license.

Melanocyte development	rab27a	evm.model.scaffold78.237;
Melanocyte development	recql4	evm.model.scaffold79.292
Melanocyte development	rnf41	evm.model.scaffold90.252;
Melanocyte development	scarb2	evm.model.scaffold155.132;
Melanocyte development	scg2	evm.model.scaffold147.42;evm.model.scaffold75.225
Melanocyte development	sf3b1	evm.model.scaffold63.23;
Melanocyte development	sfxn1	evm.model.scaffold28.394;evm.model.scaffold62.97
Melanocyte development	skiv2l2	evm.model.scaffold155.121;
Melanocyte development	slc24a5	evm.model.scaffold104.16;
Melanocyte development	slc45a2	evm.model.scaffold155.130;
Melanocyte development	snai2	evm.model.scaffold75.68;
Melanocyte development	sox18	evm.model.scaffold90.125
Melanocyte development	sox2	evm.model.scaffold23.977;
Melanocyte development	tfap2e	evm.model.scaffold79.450;
Melanocyte development	trpm7	evm.model.scaffold89.41;
Melanocyte development	tyr	evm.model.scaffold58.630;
Melanocyte development	tyrp1	evm.model.scaffold108.177;
Melanocyte development	usp13	evm.model.scaffold23.587;
Melanocyte development	vps11	evm.model.scaffold201.85;
Melanocyte development	vps18	evm.model.scaffold22.483
Melanocyte development	zic2	evm.model.scaffold63.207;
Melanocyte development, Melanosome transport	tpcn2	evm.model.scaffold110.180;
Melanogenesis regulation	asip1	evm.model.scaffold24.1152;
Melanogenesis regulation	atrn	evm.model.scaffold61.91;evm.model.scaffold61.93
Melanogenesis regulation	clcn7	evm.model.scaffold85.359;
Melanogenesis regulation	corin	evm.model.scaffold103.174;
Melanogenesis regulation	ctns	evm.model.scaffold23.51;
Melanogenesis regulation	drd2	evm.model.scaffold58.505;
Melanogenesis regulation	mc1r	evm.model.scaffold84.143;
Melanogenesis regulation	mgrn1	evm.model.scaffold80.306;
Melanogenesis regulation	myg1	evm.model.scaffold24.229
Melanogenesis regulation	nf1	evm.model.scaffold148.96;
Melanogenesis regulation	ostm1	evm.model.scaffold22.252
Melanogenesis regulation	pah	evm.model.scaffold66.283;evm.model.scaffold67.285;
Melanogenesis regulation	pomc	evm.model.scaffold18287.1;evm.model.scaffold82.36;
Melanogenesis regulation	shroom2	evm.model.scaffold23.206;evm.model.scaffold28.153;
Melanogenesis regulation	slc7a11	evm.model.scaffold109.18;

bioRxiv preprint doi: https://doi.org/10.1101/787077; this version posted September 30, 2019. The copyright holder for this preprint (which was not certified by peer review) is the author/funder, who has granted bioRxiv a license to display the preprint in perpetuity. It is made available under aCC-BY-NC-ND 4.0 International license.

Melanogenesis regulation	zeb2	evm.model.scaffold63.1009;evm.model.scaffold82.245;
Melanogenesis regulation, Components of melanosomes	rab32	evm.model.scaffold22.284;
Melanogenesis regulation, Components of melanosomes	rab38	evm.model.scaffold58.626;
Melanosome biogenesis	ankrd27	evm.model.scaffold123.74;evm.model.scaffold17829.1;
Melanosome biogenesis	ap1g1	evm.model.scaffold78.212;
Melanosome biogenesis	ap1m1	evm.model.scaffold107.226;
Melanosome biogenesis	ap3b1	evm.model.scaffold186.47;
Melanosome biogenesis	ap3d1	evm.model.scaffold23.686;
Melanosome biogenesis	bloc1s2	evm.model.scaffold23.292;
Melanosome biogenesis	bloc1s3	evm.model.scaffold58.568;
Melanosome biogenesis	bloc1s4	evm.model.scaffold79.226
Melanosome biogenesis	bloc1s6	evm.model.scaffold104.27;
Melanosome biogenesis	cd63	evm.model.scaffold90.258;
Melanosome biogenesis	dtnbp1	evm.model.scaffold79.219;
Melanosome biogenesis	fig4	evm.model.scaffold22.305
Melanosome biogenesis	gpr143	evm.model.scaffold63.395;
Melanosome biogenesis	hps3	evm.model.scaffold23.989;
Melanosome biogenesis	hps5	evm.model.scaffold27.568;
Melanosome biogenesis	kif13a	evm.model.scaffold22.1353;
Melanosome biogenesis	lyst	evm.model.scaffold28.639
Melanosome biogenesis	mlana	evm.model.scaffold155.272;
Melanosome biogenesis	nsf	evm.model.scaffold125.81;evm.model.scaffold85.138
Melanosome biogenesis	rabggta	evm.model.scaffold23.271;
Melanosome biogenesis	th	evm.model.scaffold27.193;
Melanosome biogenesis	txndc5	evm.model.scaffold45.10;
Melanosome biogenesis	vps33a	evm.model.scaffold176.125;
Melanosome biogenesis, Melanocyte development	bloc1s5	evm.model.scaffold45.11;
Melanosome transport	crh	evm.model.scaffold45.154;
Melanosome transport	dctn1	evm.model.scaffold108.42;evm.model.scaffold61.121
Melanosome transport	dctn2	evm.model.scaffold24.217;
Melanosome transport	ippk	evm.model.scaffold173.23;
Melanosome transport	map2k1	evm.model.scaffold27.524;
Melanosome transport	mlph	evm.model.scaffold63.882
Melanosome transport	myo7a	evm.model.scaffold122.10;
Melanosome transport	rab11a	evm.model.scaffold89.340;

bioRxiv preprint doi: https://doi.org/10.1101/787077; this version posted September 30, 2019. The copyright holder for this preprint (which was not certified by peer review) is the author/funder, who has granted bioRxiv a license to display the preprint in perpetuity. It is made available under aCC-BY-NC-ND 4.0 International license.

Melanosome transport	rab17	evm.model.scaffold63.881;
Melanosome transport	rab1a	evm.model.scaffold106.125;evm.model.scaffold111.24;evm.model.scaffold122.11;evm.model.scaffold135.99
Melanosome transport	rab3ip	evm.model.scaffold68.83;evm.model.scaffold69.84;
Melanosome transport	rab8a	evm.model.scaffold23.677;
Melanosome transport	ric8b	evm.model.scaffold27.301
Melanosome transport	tmem33	evm.model.scaffold86.109
Melanosome transport, Melanosome biogenesis	pmel	evm.model.scaffold24.612;evm.model.scaffold79.47;
Melanosome transport, Melanosome biogenesis	trappc6a	evm.model.scaffold58.569;
Pigment cell differentiation	cdh2	evm.model.scaffold75.131;
Pigment cell differentiation	lef1	evm.model.scaffold25.192;
Pigment cell differentiation	ovol1	evm.model.scaffold131.150;
Pigment cell differentiation, Melanocyte development	wnt3a	evm.model.scaffold75.50;
Pteridine synthesis	gchfr	evm.model.scaffold61.168
Pteridine synthesis	mycbp2	evm.model.scaffold63.234;
Pteridine synthesis	pcbd1	evm.model.scaffold165.14;
Pteridine synthesis	pcbd2	evm.model.scaffold77.416;
Pteridine synthesis	qdpr	evm.model.scaffold86.97;
Pteridine synthesis	spr	evm.model.scaffold26.365;evm.model.scaffold59.406
Pteridine synthesis, Melanogenesis regulation	gart	evm.model.scaffold82.268;
Xanthophore differentiation	ghr	evm.model.scaffold26.345;evm.model.scaffold59.333;
Xanthophore differentiation	leo1	evm.model.scaffold159.5;
Xanthophore differentiation	pax3	evm.model.scaffold147.48;evm.model.scaffold147.49;evm.model.scaffold15214.1;
Xanthophore differentiation	sox5	evm.model.scaffold65.166;

634

635 **Supplementary table 13.** KEGG pathway involved by contracted gene families

Level 1 KEGG pathway	Level 2 KEGG pathway	Number of gene family	Detail of gene family (ID)
Cellular Processes	Cell growth and death	10	2348;23;26;18;2368;1576;415;774;2156;493
Cellular Processes	Cell motility	1	5098
Cellular Processes	Cellular community-eukaryotes	4	4060;894;680;2920
Cellular Processes	Transport and catabolism	11	528;958;2678;1949;960;2065;2061;2348;2920;950;529
Environmental Information Processing	Membrane transport	2	3614;2065
Environmental Information Processing	Signal transduction	13	4381;525;894;2065;528;542;680;2156;529;5098;4490;2061;4507
Environmental Information Processing	Signaling molecules and interaction	13	4060;2061;1967;2348;611;521;525;631;616;894;1965;542;680
Genetic Information Processing	Folding, sorting and degradation	1	561
Genetic Information Processing	Replication and repair	3	2065;493;562
Genetic Information Processing	Transcription	1	493
Genetic Information Processing	Translation	4	482;497;2020;4918
Metabolism	Carbohydrate metabolism	2	2065;2061
Metabolism	Global and overview maps	9	2499;2514;2061;2065;6338;2047;2020;3783;3762
Metabolism	Glycan biosynthesis and metabolism	4	497;6338;955;3762
Metabolism	Lipid metabolism	3	3783;2514;2047
Metabolism	Metabolism of cofactors and vitamins	1	2499
Organismal Systems	Aging	1	2514
Organismal Systems	Circulatory system	2	5098;2156
Organismal Systems	Development	2	482;1949

Organismal Systems	Digestive system	7	1021;5098;2156;680;955;894;2065
Organismal Systems	Endocrine system	8	3614;4381;2156;680;2514;4490;5098;2061
Organismal Systems	Environmental adaptation	3	4490;2156;680
Organismal Systems	Immune system	23	493;1965;542;23;26;18;2301;1967;2348;4490;525;1949;4857;528;774;680;4060;529;4855;2368;12264;2565;482
Organismal Systems	Nervous system	6	2514;2061;4490;680;3783;2156
Organismal Systems	Sensory system	7	2621;2514;2617;2061;2619;680;2156

649 **Supplementary table 14.** KEGG pathway involved by size expanded gene families

Level 1 KEGG pathway	Level 2 KEGG pathway	Number of gene family	Detail of gene family (ID)
Cellular Processes	Cell growth and death	2	6680;2948
Cellular Processes	Transport and catabolism	1	2967
Environmental Information Processing	Signal transduction	3	3683;2654;6680
Environmental Information Processing	Signaling molecules and interaction	2	2654;6680
Genetic Information Processing	Folding, sorting and degradation	1	794
Metabolism	Global and overview maps	2	9457;3404
Metabolism	Glycan biosynthesis and metabolism	2	9457;3404
Organismal Systems	Development	2	1171;6680
Organismal Systems	Digestive system	1	3933
Organismal Systems	Endocrine system	1	3683
Organismal Systems	Environmental adaptation	1	2654
Organismal Systems	Immune system	1	6680
Organismal Systems	Nervous system	1	2654
Organismal Systems	Sensory system	1	546

bioRxiv preprint doi: https://doi.org/10.1101/787077; this version posted September 30, 2019. The copyright holder for this preprint (which was not certified by peer review) is the author/funder, who has granted bioRxiv a license to display the preprint in perpetuity. It is made available under aCC-BY-NC-ND 4.0 International license.

650 **Supplementary table 15.** The detail for contracted gene families.

family ID	accents KO to gene family*	function of gene family
4	-	-
112	-	-
121	-	-
127	K09228	KRAB, KRAB domain-containing zinc finger protein
139	K09228	KRAB, KRAB domain-containing zinc finger protein
148	K09228	KRAB, KRAB domain-containing zinc finger protein
149	K09228	KRAB, KRAB domain-containing zinc finger protein
276	-	-
400	K04299	P2RY14, purinergic receptor P2Y, G protein-coupled, 14
414	K05051	TAAR, trace amine associated receptor
439	K05051	TAAR, trace amine associated receptor
506	K20865	NLRP12, NACHT, LRR and PYD domains-containing protein 12
508	K22614	NLRC3, NOD3, NLR family CARD domain-containing protein 3
511	K22614	NLRC3, NOD3, NLR family CARD domain-containing protein 3
512	K22614	NLRC3, NOD3, NLR family CARD domain-containing protein 3
537	K01446	PGRP, peptidoglycan recognition protein
539	K06712	BTN, CD277, butyrophilin
556	K06751	MHC1, major histocompatibility complex, class I
557	K06751	MHC1, major histocompatibility complex, class I
603	K06499	CEACAM, CD66, carcinoembryonic antigen-related cell adhesion molecule
608	K06467	CD22, SIGLEC2, CD22 antigen
610	K06467	CD22, SIGLEC2, CD22 antigen
647	-	-
654	K12012	TRIM35, tripartite motif-containing protein 35
663	K12006	TRIM16, tripartite motif-containing protein 16
669	K12006	TRIM16, tripartite motif-containing protein 16
675	K12015	TRIM39, tripartite motif-containing protein 39 [EC:2.3.2.27]
813	K17388	ROCK2, Rho-associated protein kinase 2 [EC:2.7.11.1]
814	-	-
826	-	-
827	K17854	CYP2K, cytochrome P450 family 2 subfamily K
939	-	-
951	K08826	HIPK, homeodomain interacting protein kinase [EC:2.7.11.1]
991	K10380	ANK, ankyrin

bioRxiv preprint doi: https://doi.org/10.1101/787077; this version posted September 30, 2019. The copyright holder for this preprint (which was not certified by peer review) is the author/funder, who has granted bioRxiv a license to display the preprint in perpetuity. It is made available under aCC-BY-NC-ND 4.0 International license.

1057	K07375	TUBB, tubulin beta
1059	-	-
1100	K07377	NRXN, neurexin
1392	-	-
1492	K03654	recQ, ATP-dependent DNA helicase RecQ [EC:3.6.4.12]
1498	K06560	MRC, CD206, CD280, mannose receptor, C type
1502	-	-
1505	K06560	MRC, CD206, CD280, mannose receptor, C type
1518	K11275	H1_5, histone H1/5
1519	K11252	H2B, histone H2B
1521	K11253	H3, histone H3
1522	K11251	H2A, histone H2A
1533	K18626	TCHH, trichohyalin
1554	K05096	FLT1, VEGFR1, FMS-like tyrosine kinase 1 [EC:2.7.10.1]
1567	K06634	CCNH, cyclin H
1592	K16826	SIRPB2, signal-regulatory protein beta 2
1593	K16826	SIRPB2, signal-regulatory protein beta 2
1597	K10784	TRAV, T cell receptor alpha chain V region
1599	K06553	VPREB, CD179a, pre-B lymphocyte gene
1600	K06856	IGH, immunoglobulin heavy chain
1601	K06856	IGH, immunoglobulin heavy chain
1611	K06554	IGLL1, IGLL, CD179b, immunoglobulin lambda-like polypeptide 1
1613	K06553	VPREB, CD179a, pre-B lymphocyte gene
1614	K10785	TRBV, T-cell receptor beta chain V region
1634	K09228	KRAB, KRAB domain-containing zinc finger protein
1659	K04257	OLFR, olfactory receptor
1664	K04257	OLFR, olfactory receptor
1666	K04257	OLFR, olfactory receptor
1769	K19470	C1QTNF6, complement C1q tumor necrosis factor-related protein 6
1807	K06238	COL6A, collagen, type VI, alpha
2057	-	-
2080	-	-
2117	K01068	ACOT1_2_4, acyl-coenzyme A thioesterase 1/2/4 [EC:3.1.2.2]
2142	K04615	GABBR, gamma-aminobutyric acid type B receptor
2146	K22611	SART3, TIP110, squamous cell carcinoma antigen recognized by T-cells 3

bioRxiv preprint doi: https://doi.org/10.1101/787077; this version posted September 30, 2019. The copyright holder for this preprint (which was not certified by peer review) is the author/funder, who has granted bioRxiv a license to display the preprint in perpetuity. It is made available under aCC-BY-NC-ND 4.0 International license.

2159	K16810	TBCCD1, TBCC domain-containing protein 1
2200	K18543	HCE, choriolysin H [EC:3.4.24.67]
2614	K14480	APOL, apolipoprotein L
2787	K06719	CD300, CD300 antigen
3054	K06556	CD200, CD200 antigen
3071	K06733	SLAMF7, CD319, SLAM family member 7
3082	-	-
3084	-	-
3480	K05039	SLC6A6S, solute carrier family 6 (neurotransmitter transporter, GABA) member 6/8/11/12/13
3550	-	-
3561	-	-
3620	-	-
3651	K18684	ALOXE3, hydroperoxy icosatetraenoate dehydratase/isomerase [EC:4.2.1.152 5.4.4.7]
3796	K05152	TNFRSF14, HVEM, CD270, tumor necrosis factor receptor superfamily member 14
3883	-	-
3919	K06087	CLDN, claudin
4277	-	-
4321	K13826	HBZ, hemoglobin subunit zeta
4384	-	-
4401	K17072	IFI47, interferon gamma inducible protein 47
4503	K21922	KCTD21, BTB/POZ domain-containing protein KCTD21
4741	K04612	CASR, calcium-sensing receptor
4743	K04612	CASR, calcium-sensing receptor
4827	K11170	DHRSX, dehydrogenase/reductase SDR family member X [EC:1.1.-.-]
4846	K06554	IGLL1, IGLL, CD179b, immunoglobulin lambda-like polypeptide 1
6363	K03663	FUT9, 4-galactosyl-N-acetylglucosaminide 3-alpha-L-fucosyltransferase [EC:2.4.1.152]
7663	K14217	IFIT1, interferon-induced protein with tetratricopeptide repeats 1
11586	-	-
11850	-	-
11970	K14639	SLC15A5, solute carrier family 15, member 5
12008	K09228	KRAB, KRAB domain-containing zinc finger protein
12055	K03985	PLAUR, CD87, plasminogen activator, urokinase receptor